4/22/65

NASA TECHNICAL NOTE

NASA TN D-2760

NASA TN D-2760

MEASUREMENT OF OPTICAL RADIATION FROM THE WAKE OF ABLATING BLUNT BODIES IN FLIGHT AT SPEEDS UP TO 10 KM PER SECOND

by Jack D. Stephenson

Ames Research Center
Moffett Field, Calif.

NATIONAL AERONAUTICS AND SPACE ADMINISTRATION • WASHINGTON, D. C. • APRIL 1965

NASA TN D-2760

MEASUREMENT OF OPTICAL RADIATION FROM THE WAKE OF ABLATING BLUNT BODIES IN FLIGHT AT SPEEDS UP TO 10 KM PER SECOND

By Jack D. Stephenson

Ames Research Center
Moffett Field, Calif.

NATIONAL AERONAUTICS AND SPACE ADMINISTRATION

For sale by the Clearinghouse for Federal Scientific and Technical Information
Springfield, Virginia 22151 – Price $2.00

MEASUREMENT OF OPTICAL RADIATION FROM THE WAKE OF ABLATING BLUNT BODIES IN FLIGHT AT SPEEDS UP TO 10 KM PER SECOND

By Jack D. Stephenson
Ames Research Center

SUMMARY

[Optical wavelength radiation from the wakes of small gun-launched models (spherically blunted bodies) has been measured at speeds from 5 to 10 km/sec and at stream densities from 0.001 to 0.2 atmosphere. Results indicate that radiation in the wavelength range, 0.2 to 1.0 micron, is caused primarily by the presence of ablation material in the wake. The radiation intensity and spectral quality differ considerably among the various plastic materials tested (a polycarbonate, polyethylene, an epoxy, and polymerized formaldehyde).

For conditions at which a majority of the data were obtained, the peak radiant intensity from the wake varied directly with stream density and approximately with the 7.5 power of the flight velocity.]

The variation of intensity of the wake radiance with downstream distance along the wakes of polycarbonate models, following the region of peak intensity, could be approximated by exponential decay functions. The decay rates varied with the square root of the stream density.

When the intensity of the wake radiation is high, the radiative heat load on the body base can be significant. Results of calculations of heating rates on the model base are presented and relations for scaling heating rates are discussed.

INTRODUCTION

Thermal, visible, and ultraviolet radiation from flow fields of hypervelocity bodies has been extensively studied recently because of its contribution to the heating of high-speed entry bodies and because of its possible use in tracking entry vehicles. Measurement of the radiative intensity and its geometric distribution has also been a valuable aid in the understanding of various details of the flow around hypersonic bodies (ref. 1). Because some evidence indicates that the occurrence of bright luminous wakes is associated with a dense electron population, information showing intensity and distribution of wake radiance may be useful in conjunction with microwave scattering experiments (ref. 2).

Although some information on the spectral and geometric characteristics of wake radiation from large-scale ablating bodies can be obtained from photographic and radiometric observations of their flight into the atmosphere, it is not economically feasible to conduct large numbers of such experiments, and when they are made, results can be difficult to evaluate because of the necessarily large distances of the instrumentation from the entry trajectory.

Many characteristics of radiating wakes can not be predicted well from theory, because such predictions require the solution of a combination of complex problems: determination of transition locations, chemistry and reaction rates of high enthalpy reactions, ionization effects, and radiative properties of the species involved. Some wake characteristics have been the subject of theoretical investigations by various authors. References 3, 4, and 5 present studies aimed at the prediction of thermal properties, pressures, degree of ionization, and the effect of distance on the lateral extent of the wake region, and reference 3 includes results of wake-radiation calculations for a nonablating body.

During a test program initiated at Ames Research Center to study radiative heating from shock layers of small gun-launched models in flight at speeds ranging from 5 to 10 km/sec and at free-stream densities from 0.001 to 0.2 atmosphere, the wake radiation was also measured. The shock-layer results have been described in references 6 and 7, which report studies of radiation from air in the gas cap, and references 8 and 9, which present results of tests to determine the effects on radiative heating of ablation products in the gas cap.

The purpose of the present report is to present and correlate the wake observations. Predictions (based on the experimental data) of scale effects on radiative heating of the afterbody and on spectral power emitted by wakes are included.

SYMBOLS

A_p effective ablation area, cm^2

A_w cross-section area of viscous wake, cm^2

B stagnation-point velocity gradient factor

D body diameter, cm

H_{eff} effective heat of ablation, watt sec/g

I radiant power per unit volume, $watts/cm^3$

I_b integral appearing in equation (A15)

K exponential decay factor

$\dot{m}$	ablation mass rate, g/sec cm^2
$\dot{M}_B$	mass flow in boundary layer, g/sec
$\dot{M}_W$	mass flow in wake, g/sec
p	pressure, mm Hg
P	radiative power, watts
P_S	similarity parameter
$\dot{q}$	radiative heat flux, watts/cm^2
R	body radius of cross section, cm
R_N	nose radius, cm
$\Re$	gas constant
T	temperature, ^oK
u	local velocity parallel to surface, km/sec
U_∞	free-stream velocity, km/sec
v	velocity normal to surface
U_W	velocity of wake relative to body, km/sec
W	radiative power from a length of wake equal to the body diameter, watts
W_λ	spectral power, watts/micron
x	axial distance of point in wake behind model base, cm
Z	compressibility
Γ	factor defined by equation (A30)
ζ	exponent defined by equation (A30)
λ	wavelength, microns
μ	absolute coefficient of viscosity, g/cm sec, also microns
ξ	exponent defined by equation (A30)
ρ	density, g/cm^3
σ	scale factor, R_L/R_M

Subscripts

b	base of body
e	edge of boundary layer
g	forebody shock layer (gas cap)
L	large scale
M	small or model scale
P	ablation product
w	wake
W	wall
o	at location of peak radiance
∞	free stream

EXPERIMENTAL APPARATUS

Facility

The tests were conducted in the Pilot Hypervelocity Free-Flight Facility of Ames Research Center. The facility, shown schematically in figure 1, is a countercurrent device in which 7.1-mm-diameter models are launched with a light-gas gun through an instrumented shock-tube wind-tunnel test section containing either an opposing air stream having a Mach number of 6, or still air. Reservoir conditions for the test-section nozzle are provided by a cold-helium-driven shock tube operated under tailored interface conditions. Most of the data presented herein were obtained under still-air conditions at velocities up to 8 km/sec. The 1.8 km/sec opposing air stream was used for higher velocities, approximately to 10 km/sec. References 6 and 10 describe the characteristics of the facility. Model velocity, attitude, and position were determined with conventional ballistic-range instrumentation - spark shadowgraphs and electronic counters. Properties of the hypersonic air stream were determined from measurements of shock velocity and transient pressures in the shock tube and static pressures on the test-section wall.

Radiometers

Radiation was measured with an array of 8 to 10 radiometers consisting of photomultipliers and optical filter combinations with spectral responses, as shown in figure 2 and as given in the table below.

Wavelength of maximum sensitivity, micron	Half-amplitude band pass, micron
0.235	0.049
.265	.049
.312	.056
.369	.038
.460	.026
.518	.059
.545	.060
.640	.077
.758	.071
.920	.175

The radiometers were mounted around the test section at right angles to the model flight path, as illustrated in figure 1. Figure 3 shows the geometric arrangement of a typical radiometer, including the slit pair which determines the field of view in the direction of flight. The voltage outputs of the photomultipliers are displayed on oscilloscopes and photographed, providing a record of the radiation as a function of time.

Cameras

Direct photographs of the luminous flow were obtained with image-converter cameras having S-11 photocathode responses and with a camera employing a Kerr-cell shutter. Exposure times were typically 0.05 μsec. The photographs aided in the interpretation of some of the radiometric data and were useful for detemining the spatial extent of the luminosity and the presence of turbulence of the wake.

Models

The models were made of the following plastic materials: Lexan (a General Electric Company polycarbonate), high-density polyethylene, G. E. 124 (an epoxy material designed to form a char), Teflon (a DuPont polytetrafluoroethylene), and Delrin (a polymerized formaldehyde also made by DuPont). Most of the models had spherical-segment forward faces of 0.5 cm radius and short cylindrical afterbodies, as depicted in figure 4. The Teflon models had tapered afterbodies so that they could be launched in sabots, because without a sabot Teflon was not strong enough to withstand the launching accelerations. Sketches of a Teflon model and a sabot are also shown in figure 4.

DATA REDUCTION

The total radiant flux from the source per unit wavelength (watts per micron) per unit length of the wake, in the wavelength band to which the radiometer is responsive, was deduced from the radiometer outputs. The relations between the radiometer outputs and the source power per micron were obtained by calibration, as described in reference 6. The axial length of the region viewed by each radiometer was computed from the known width and geometric arrangement of the viewing slits, and with this dimension the power emitted by a length of wake equal to the body diameter was calculated. Most of the radiometer data are presented in terms of this length.

RESULTS

A typical set of radiometer records is shown in figure 5(a). The signal produced by the gas-cap region of the model, as it moved into and out of view, is readily identified as a short (2 μsec) initial pulse. It is followed by a signal of longer duration representing the wake radiation variation with time (i.e., distance) behind the model, first increasing (in this example), and then more gradually decaying. In some tests the wake radiation was at a maximum immediately behind the gas cap and then decreased more or less continuously.

Figure 5(b) shows a typical image-converter photograph of the luminous regions around a model in flight. In this example, the material is polycarbonate, velocity is 6.6 km/sec, and density is 0.072 times atmospheric.

Spectra of Wake Region of Maximum Luminosity

The oscilloscope data from the radiometers were analyzed to determine the spectra of the wake radiation at the location of maximum brightness. When the oscilloscope trace did not exhibit a distinct peak in the wake, the maximum was assumed to be the value recorded at the time just after the bow shock layer went out of the field of view.

Effect of model material.- Examination of the intensity and spectral characteristics of the peak wake radiance indicates that the model material is of major importance. This is shown in figure 6, which presents a comparison of spectra obtained with models made of polycarbonate, polyethylene, G. E. 124, polyformaldehyde, Teflon, and aluminum. The observed spectral radiation into 4π steradians in watts per micron per model diameter is plotted as horizontal lines, the lengths of which indicate the 50-percent band-pass widths of the radiometers; a curve is then faired through these lines to approximate the spectrum.

It is evident that the wakes of the polycarbonate models were much brighter than those for models made of the other materials. For three of the

materials shown, a large fraction of the emitted power within the response range of the radiometers is in the infrared part of the spectrum.

Caution must be exercised when comparing some of the results since test velocities were not all the same. The effect of correcting for the spread in velocities would be to exchange the relative positions of the polyformaldehyde and Teflon data, for example.

Figure 6 shows that with aluminum, Teflon, and polyformaldehyde models, the wake radiation was of very low intensity. As a result, the accuracy of the measurements is poor compared with that when the wakes were bright. Inaccuracies are due to the difficulty of specifically identifying the wake contribution, as distinguished from the reflections from the test-section walls of the much brighter gas-cap radiation. Although the magnitude of these additional radiometer signals is not known, the effect is small for bright wakes but can be significant when the wake intensity is very low.

Figure 6 indicates that the aluminum model, the velocity of which was 6.2 km/sec, had a brighter wake than the polyformaldehyde model. Calculations have indicated that transient aerodynamic heating of the aluminum model after launching would not be sufficient to initiate ablation (see, e.g., ref. 11). A possible conclusion from this is that (if in fact the model were not ablating) the observed wake is the result of air radiation. If this is true, it implies that the ablation of the polyformaldehyde models attenuates the air radiation. In general, however, these results, from tests in which the wake radiance was very weak, must be considered as tentative because of the poor signal-to-noise ratio of the measurements.

The data in figure 6 for the three materials producing low wake intensities are probably only useful to indicate upper limits of spectral power at a given wavelength since sources other than the wake may be significant.

Effect of stream density on peak spectra.- The effect of varying the free-stream density from 0.001 to 0.18 atmosphere on the spectra of the peak wake radiation observed behind polycarbonate and polyethylene models is shown in figure 7. When the spectra are compared, the fact that the model velocities differ (ranging from 5.9 to 7.4 km/sec) must be kept in mind, as mentioned before. At the higher densities, a major part of the radiant power is in the infrared but with decreasing density it shifts toward the visible. At the lowest density, 0.001 atmosphere, for which data were obtained only with polyethylene, the fraction in the infrared again increases, resulting in a relatively uniform distribution throughout the wavelength range.

The previously mentioned uncertainty (in the data for wakes that show low radiation) resulting from the effects of bright gas caps influencing the radiometer readings, also is present in the data of figure 7 at short wavelengths. At these wavelengths, the wakes have relatively low radiant power, whereas, the gas-cap power is high (ref. 6). Thus, the uncertainty is a larger fraction of the measurements in the ultraviolet and short wavelengths than in the visible and infrared.

Integrated Peak Radiative Intensity

Effect of ambient air density.- The peak radiation spectra have been integrated to obtain the total power (watts/diameter) in the wavelength range of the radiometric measurements (0.2 to 1.1 micron). This integrated power is plotted in figure 8 as a function of ambient density for several velocities. Since the model velocities in general differed from the nominal values shown in the figure, the data were adjusted using a 7.5 power variation of the radiation with velocity. The basis for choosing this power will be remarked upon later.

Figure 8(a) presents the radiated power as a function of density for three materials - polycarbonate, polyethylene, and G. E. 124 - at a model velocity of 6.7 km/sec. The data for all of these materials show that the radiant power is essentially proportional to the ambient density. There is a fairly large random spread in the data which is believed to result primarily from an inherent unsteadiness of the wake luminosity rather than from a lack of precision of the measurements. This statement is based on the fact that the repeatability of the measurements of gas-cap radiative intensities is much better than that of peak wake radiative intensities. The one data point in figure 8(a) for a polyformaldehyde model is interpreted as representing an upper limit deduced from the data as was mentioned before (cf. fig. 6).

Results obtained at higher velocities, figure 8(b), are generally similar to those at 6.7 km/sec.

Effect of velocity.- In figures 9(a) and 9(b) the peak wake integrated radiative intensity is presented as a function of model velocity in logarithmic coordinates for polycarbonate and polyethylene models at several ambient densities. Included on the figure is a line representing a 7.5 power variation with velocity. The lack of more extensive experimental data prevents precise determination of velocity dependence; however, at velocities up to 7 km/sec for polycarbonate models, and for all the data obtained with polyethylene models (except perhaps for the lowest density), the wake intensity varies as velocity raised to a power between 7 and 8.[1] At velocities above 7 km/sec, one data point for polycarbonate indicates a more gradual variation.

Radiance Downstream From Peak Region

Spectra at various distances behind the model, up to 30 model diameters, were obtained from the oscilloscope records. Such spectra for polycarbonate, polyethylene, and G. E. 124 models are shown in figure 10. Results shown for a stream density of 0.072 atmosphere indicate little change in spectral quality with distance; the intensities at all wavelengths decrease smoothly at about the same rate. At a lower density, 0.006 atmosphere, with polycarbonate, there was a generally uniform decrease with distance at the longer wavelengths (above 0.55 μ) but at short wavelengths the decay rate was

[1]An exponent of 7.5 was chosen for adjusting the data presented in figure 8 (to account for velocity variations), but choosing a different value between 7 and 8 would not change the results significantly.

erratic. With polyethylene and G. E. 124 at low stream densities (0.009 atmosphere and 0.018 atmosphere, respectively) variations in the spectral distribution with distance can be observed. With polyethylene, this variation consists of an increase in the relative prominence of a band near 0.52 μ and a decrease in the contribution of a bright band near 0.37 μ. With G. E. 124, the radiation at wavelengths above 0.5 μ has a considerably decreased contribution at the larger distances.

The spectra obtained in the tests do not have sufficiently high wavelength resolution for precise identification of the excited species producing the observed radiation. However, figure 10 appears to show some strong band structure. Undoubtedly, an important part of the radiation from wakes of these ablating plastic models is related to the presence of a substantial amount of carbon in some form resulting from the thermal decomposition of the plastics. The spectra for polycarbonate show a strong band in the neighborhood of 0.5 μ, which is probably attributable to the C_2 Swan system. The intensity of this system at low density and a velocity of 7.5 km/sec (fig. 10(a)) shows only a slight decay with distance up to 10 diameters and then a much more rapid decay rate. At higher density, the decay rate is relatively uniform up to a distance of 20 diameters. For polyethylene, figure 10(b) indicates that this band system is strong and increases with distance up to 20 diameters at low ambient densities, but at a higher density (0.072 atmosphere) it is not prominent at any location.

An intense system is evident in the spectra for polyethylene in the wavelength band near 0.37 micron. This may be the CN violet system (0.388 micron). Comparing figure 10(b) with figure 7(b) shows that this band intensity was considerably influenced by a variation in velocity, becoming quite weak with a decrease in velocity from 7.2 to 6.1 km/sec at a stream density of 0.072 atmosphere. The CN violet also appears to contribute importantly (but with less relative prominence than for polyethylene) to the total power in the spectra for G. E. 124 (fig. 10(c)) and at an ambient density of 0.006 atmosphere to the power in the spectra for polycarbonate (fig. 10(a)).

Throughout the range of densities of the tests, the decay to half amplitude of the luminosity of wakes from polycarbonate and G. E. 124 models could generally be approximated by an exponential decay function. (This has also been pointed out in ref. 1.) A damping coefficient K has been calculated, assuming that the decay of luminosity can be represented by the relation

$$W = W_1 e^{-K\left(\frac{x}{D} - \frac{x_1}{D}\right)} \tag{1}$$

where x_1 is the distance to the start of the decay, W_1 is the radiant power per unit length of the wake at the start of the decay, and D is the model diameter. From a comparison of the damping coefficients obtained from the outputs of the various radiometers, it can be determined whether the decay rates depend on wavelength. Figure 11 shows, as functions of stream density, values of K obtained from oscilloscope records from three radiometers responsive to the following wavelength intervals: a broad band in the ultraviolet and visible (0.21 to 0.6 micron), a narrower band in the visible (0.48 to 0.56 micron), and a band in the near infrared (0.8 to 1.1 microns). The

three plotted curves, which each represent averages of results from 24 tests, indicate that at all three wavelength bands the decay rate increased approximately with the square root of the stream density and that at the different wavelengths the decay rates were not greatly different.

When the radiometer data obtained in tests of polyethylene models were used with equation (1) to calculate damping coefficients, it was found that these coefficients varied erratically both with density and with wavelength. This behavior of the decay rate is probably associated with other anomalies that were observed in the streamwise variation of the wake radiance of the polyethylene models, which are discussed in the following section.

Variations in the Location of Peak Radiance

In tests with polyethylene models, at the highest and lowest densities studied, the wake intensity was observed to be a maximum immediately behind the location of the gas cap and to decay monotonically thereafter. At densities between these extremes, there were large variations in the location of peak luminosity. These are illustrated in figure 12, where the wake radiation measured by one radiometer, sensitive to wavelengths from 0.45 to 0.59 micron, is plotted as a function of distance. The peak wake intensity is considerably farther to the rear at densities of 0.01 and 0.02 than at higher and lower densities.

It can be reasoned that the varying location of peak brightness may be related to a variation in the characteristics of the viscous flow (separated boundary layer) and involves the rate of turbulence growth. From this reasoning, it was believed that a correlation of the data, based on Reynolds number, might be possible. For this correlation to be shown by experimental results, it is necessary to include the variation of more than the single variable density. Results from tests of larger models (diameter = 1.52 cm) were available. These results are shown in figure 13 together with the results from the present tests, as functions of Reynolds number based on free-stream conditions. The figure indicates that as the Reynolds number decreased to about 25,000, the luminous peak moved rearward. At lower Reynolds numbers, the peak is very near the body. It should be remarked, however, that for these conditions it is quite possible that a second peak intensity point existed in the wake at large values of x/D, where the wake was not scanned.

Also included in the figure are results from reference 12 showing as a function of Reynolds number the location in the wake at which transition was judged to occur on the basis of the appearance of eddies in schlieren photographs. The similarity of conditions at which these two phenomena occur suggests that they are related, but further study is required to ascertain whether this apparent relationship is real or fortuitous. The results reported in reference 12 were for a much lower velocity - 2.6 km/sec - as compared to 6.7 for the tests reported herein.

An image-converter photograph obtained during the present tests (fig. 14) shows some of the details of the luminous wake at a Reynolds number of 68,400

(ambient density, 0.02 atmosphere). The region in the wake where the diameter appears to increase as a result of large-scale turbulence coincides with the location of peak intensity measured with the radiometer previously shown on figure 13.

Wake and Gas-Cap Radiation Compared

The optical radiation emanating from the entire heated flow field surrounding a hypersonic body entering the atmosphere is important in locating, identifying, and tracking the body. In this application, the photometric observations would usually be made from a great distance, so that, because of limitations in the spatial resolving power of the photometric instrumentation, it may be impossible to examine separately the characteristics of the gas cap and the wake regions. For this reason it is useful to know how the radiant power from the two regions compare. Several variables are involved in such a comparison, including the effect of the differences in shape and extent of the luminous regions, and the effect of ablation-product radiation originating in the gas cap. As a preliminary step, comparing the radiant power from the wake with the calculated power radiated from equilibrium air in the gas cap gives a concept of the relative contribution of the wake. The air radiation values were obtained from reference 13.

The power from the gas cap can be computed by integrating the calculated local distribution of power throughout the shock layer, as discussed in reference 6, but in the calculations discussed here, it was obtained by computing stagnation-point radiation and applying a correction factor to account for radiation distribution in the shock layer. Values of the correction factors were estimated by the method discussed in reference 14.

The wake radiation was calculated from the integral

$$P_W = \int_0^\infty E(x)dx \tag{2}$$

where $E(x)$ is power per centimeter of wake length. The value of E is assumed a constant (E_0) for a short distance (x_1) behind the body, decaying exponentially thereafter. Then equation (2) becomes

$$P_W = E_0 x_1 + E_0 \int_{x_1}^\infty e^{-K'(x-x_1)} dx \tag{3}$$

where K' is the damping coefficient, K, mentioned earlier, divided by the body diameter.

The ratio of the integrated wake output to the output from equilibrium air in the gas-cap volume is presented in figure 15 as a function of ambient density for polycarbonate models at two velocities, 6.7 and 9.7 km/sec. It is seen that the wake power is much greater than that of the gas cap, its relative contribution becoming larger with decreasing density.

Two factors should be taken into account in the interpretation of figure 15; both result from the assumption that all the gas-cap radiation is the radiation from air in thermodynamic equilibrium. First, at the lower densities at which the tests were conducted, the shock-layer air was not in equilibrium and measured shock-layer radiative intensities are greater than those calculated for equilibrium conditions. These measured values are discussed in reference 6. The second factor is that for conditions for which the wake intensity is high, there is also a significant increase in gas-cap radiation due to the presence of ablation products in the shock-layer region. This effect, which is discussed in detail in reference 8, would reduce the ratios shown in figure 15 at all of the test conditions indicated. It should also be noted again that the wakes of polycarbonate models were the most luminous of any of those measured experimentally.

APPLICATION TO FULL SCALE

The data and correlations presented thus far apply to the small-scale models that were tested. Applying the results to problems of predicting radiation intensity from wakes of large bodies entering the atmosphere requires consideration of the effect of scale. Appendix A is an attempt to predict peak intensity radiation at large scale on the basis of present data. The following assumptions are made:

1. The radiant intensity is assumed to be a function of only temperature, mass density of the material ablated from the body, and mass density of the air comprising the wake flow.

2. It is assumed that the region from which radiation emanates is uniform in temperature, pressure, and chemical composition across each section because its components are completely mixed; these properties may vary along the wake, however.

3. The cross-section area of the viscous wake is assumed to be determined by the wake velocity and by the density of the mixture of ablation-product gas and air from the boundary layer.

A scaling relation is first derived for bodies of different size at a given, constant free-stream density. In a second derivation, Reynolds number is held constant by changing density in inverse proportion to scale. When density is held constant and the size changes, the Reynolds number varies, and so the flow geometry is expected to vary. Which one of these two relations is chosen in a particular calculation depends on whether the fluid mechanics or the chemistry of the flow is expected to dominate the scale effect. If the location of boundary layer or wake transition and the degree of turbulence in the wake have significant effects on radiation, or if the wake emissivity is so high that the wake can not be considered optically thin, data obtained in tests conducted at full-scale Reynolds number provide a better basis for scaling. Such tests can also duplicate nonequilibrium flow characteristics in the shock layer, where binary collision processes tend to predominate. Scaling at constant density permits the duplication of

high-enthalpy chemical reactions involved in the boundary layer and wake flows but does not simulate nonequilibrium effects in either the shock layer or expansion regions.

Constant Density, Variable Size

The analysis in appendix A for the case where free-stream density is held constant indicates that the peak wake radiant power per unit volume (watts/cm^3) is invariant with change in body size, $I = I_M$, while the wake radius at the location of this peak radiance relative to the body radius varies as follows, from equation (A25)

$$R_W/R \propto R^{-1/4}$$

In obtaining these results it was assumed that the local pressure in the wake was not affected. The scaling relation is restricted to variations in scale within which the wake flow does not undergo a major change in its characteristics, such as a change from a long laminar run to one with laminar-to-turbulent transition near or on the body. An examination of photographs of luminous wakes of models indicates that there is a large range of Reynolds numbers in which such a major change does not take place.

Experimental evidence that the relative wake diameter varies with the $-1/4$ power of the Reynolds number is shown in figure 16 with luminous wake measurements taken from photographs obtained with image-converter cameras and a Kerr-cell shuttered camera.

Constant Reynolds Number

The second analysis presented in appendix A furnishes a means of calculating peak radiative intensity of a wake behind a large body on the basis of data from tests of small models at the same Reynolds number. The following relation, expressing the effect of scale on the peak radiative intensity (power per unit volume), is derived for a flight velocity of 6.7 km/sec:

$$I, \text{ watts/cm}^3 \propto R^{-3/2} \qquad (4)$$

The exponent on R was obtained from the experimental data; hence, it should not be expected to apply generally to other materials, flight speeds, etc. The appendix also indicates that there is flow similarity, except for density-dependent chemical effects. The effect of scale on the longitudinal distribution of the radiation is not known.

BASE HEATING FROM WAKE RADIATION

The wake is a source of radiant heating of afterbody surfaces. In the following paragraphs, relations are developed for this heating rate both for the models of the present tests and for full-scale vehicles.

The total radiant power from an optically thin wake segment of length dx is

$$dP = \pi R_w^2 I(x)\,dx \tag{5}$$

where $I(x)$ is the power radiated from a unit volume in the wake. The wake is assumed to be a line source of radiation, the strength of which varies along its length. The average radiant flux intercepted by a body base of radius R_b at the distance x is

$$d\dot{q}_b = \frac{\Omega dP}{4\pi^2 R_b^2}, \text{ watts/cm}^2 \tag{6}$$

where Ω is the solid angle intercepted by the base. (To obtain the actual heating rates, equation (6), of course, would necessarily include the surface absorptivity.) The solid angle is given by

$$\Omega = 2\pi \left[1 - \frac{x}{\left(R_b^2 + x^2\right)^{1/2}} \right]$$

To calculate the heating produced by all of the wake, equation (6) is integrated over the wake length:

$$\dot{q}_b = \frac{1}{2} \int_o^\infty \left\{ \frac{R_w^2 I(x)}{R_b^2} \left[1 - \frac{x}{\left(R_b^2 + x^2\right)^{1/2}} \right] \right\} dx \tag{7}$$

Base Heating of Model

When equation (7) is used to calculate base heating, it can be shown that this heating depends primarily on radiation emitted from the wake close to the body and that, among the wakes observed in the tests, differences in the longitudinal distributions of wake radiation are of only secondary importance. Large variations in this distribution, representing the entire range of distributions observed in the tests for which wake intensities were high, had only a small effect on the heating. For this reason, a single distribution function, which approximated the measured distributions, was used to calculate base heating of the model at all stream densities. This

distribution consisted of a region in which the radiation (watts per cm length) increased linearly from a value of 0.9 times the maximum at the body base to a maximum at 1.3 diameters behind the body, followed by a region of linear decrease to 50 percent of the maximum at a distance of 10 diameters. With this distribution and the peak intensities shown in figure 8, equation (7) gives the base heating rates for polycarbonate models of 0.71 cm diameter tabulated below. The ordinate W (fig. 8) is related to I_o, the maximum value of the parameter I (eq. (7)), by the formula

$$I_o = \frac{W}{\pi R_w^2 D}$$

ρ_∞/ρ_o	W (fig. 8)	$\dot{q}_b$, watts/cm^2
0.003	1.5	1.4
.009	4.4	4.2
.018	9.4	9.0
.072	37.2	35.5
.180	90.7	87.0

Base Heating at Large Scale

In order to examine the effect of scale on base heating, equation (7) is written in dimensionless form as follows, where R is a characteristic body radius,

$$\dot{q}_b = \frac{1}{2} R \int_o^\infty \frac{(R_w/R)^2 I(x/R)}{(R_b/R)^2} \left\{ 1.0 - \frac{x/R}{[(R_b/R)^2 + (x/R)^2]^{1/2}} \right\} d\left(\frac{x}{R}\right) \qquad (8)$$

Expressing the radiant intensity as

$$I\left(\frac{x}{R}\right) = I_o \left[\frac{I(x/R)}{I_o}\right]$$

and assuming $R_b = R$, equation (8) is

$$\dot{q}_b = \frac{1}{2} \frac{R_w^2 I_o}{R} \int_o^\infty \left[\frac{I(x/R)}{I_o}\right] \left\{ 1.0 - \frac{x}{R}\left[1 + \left(\frac{x}{R}\right)^2\right]^{-1/2} \right\} d\left(\frac{x}{R}\right) \qquad (9)$$

It has previously been indicated that for the calculation of base heating it is necessary to know the longitudinal distribution of wake radiation in the near wake only. The effect of scale on this distribution has not been determined; however, in tests of the model, it was observed that a single distribution would adequately represent the distribution throughout a large Reynolds number range. In the absence of better information, and because it

can be shown that small variations in the distribution do not greatly affect the base heating results, it is assumed that this distribution, described in the preceding section, also applies at large scale. Then the integral of equation (9) is independent of size, and the entire effect of scale is included in the geometry factors and the value of the peak radiation I_o, which can be calculated by means of the scaling rules already discussed.

If the radiative heating of the large-scale body is to be determined by extrapolating from tests at the same density and velocity, I_o is constant and, according to equation (A25), the wake radius varies with the 3/4 power of the scale. Inserting these relations in equation (9) and denoting the integral in equation (9) by Λ gives

$$\dot{q}_b \propto \frac{(R^{3/4})^2}{R} I_o \Lambda \propto R^{1/2} I_o \Lambda \tag{10}$$

$$\dot{q}_{b_L} = \sigma^{1/2} \dot{q}_{b_M} \tag{11}$$

If an extrapolation of data is based on tests at the same Reynolds number, at a velocity of 6.7 km/sec, the wake intensity dependence is expressed by equation (4) for the materials studied in the present tests. Hence,

$$I_L = I_M \sigma^{-3/2}$$

From this, equation (9) gives the scaling rule

$$\dot{q}_{b_L} = \sigma^{-1/2} \dot{q}_{b_M} \tag{12}$$

Example of Scale Effect

The result of applying the above scaling relation is illustrated with the following example. Assume a scale factor of 60, which for constant Reynolds number corresponds to a body radius of 21.3 cm. For flight of this large body at a stream density of 0.003 atmosphere, the previously given radiative heating rate that was calculated for the model at a stream density of 0.18, 87 watts/cm^2, is used. Then the radiative heating of the base of a large body similar in shape to the model is obtained from equation (12).

$$\dot{q}_{b_L} = \dot{q}_{b_M} \sigma^{-1/2} = (87)(60)^{-1/2}$$

$$= 11.2 \text{ watts/cm}^2$$

CONCLUSIONS

Results of ballistic tests of small-scale ablating models at speeds up to 10 km/sec have been analyzed and indicate the following conclusions relevant to the characteristics of their luminous wakes.

1. Essentially all of the measured optical radiation from the wake is produced by the effects of material ablated from the model. The wakes of models made of polycarbonate were considerably brighter than those of other materials.

2. The radiative intensity of the region in the wake where the brightness was a maximum generally varied directly with free-stream density at fixed model velocities.

3. The rate at which the luminosity decayed with distance behind the model varied approximately with the square root of the stream density.

4. The integrated power radiated from all the polycarbonate model wakes was about one order of magnitude greater than that calculated for all the equilibrium air in the shock layer at the highest test free-stream densities and about three orders greater at the lowest test densities.

5. It was deduced from the present results that afterbody heating from wake radiation is mostly contributed by the near wake, usually that portion of the wake within ten body diameters. At constant stream density, the heating rates are predicted to increase as the square root of the scale, and at constant Reynolds number (for a velocity of 6.7 km/sec), the heating rates are predicted to vary inversely with the square root of the scale.

Ames Research Center
National Aeronautics and Space Administration
Moffett Field, Calif., Dec. 18, 1964

APPENDIX A

SCALE EFFECT ON RADIATIVE INTENSITY

In this appendix, the effect of scale on peak wake radiative intensity is estimated, on the basis of calculated effects of scale on wake properties and on concentration of gaseous ablation products. It is assumed that the radiation is emitted by an inner viscous core containing the air and ablated material from the boundary layer. Effects of scale on wake properties can, to a large degree, be traced to and correlated with effects in the boundary layer. For this reason, the analysis will first consider the boundary-layer flow.

Because most of the ablation is from the forebody, the boundary layer on only this part of the body is assumed to contribute significantly to the wake core. Other assumptions are that (1) the boundary layer is laminar; (2) the wall temperature is constant, fixed by the sublimation temperature of the surface material; and (3) the ablation mass injected is gaseous with state and transport properties identical to equilibrium air. The boundary-layer analysis is based on solutions presented in references 9 and 15. Reference 15 shows that the differential equations (motion and energy) for a two-dimensional stagnation-flow boundary layer with flow through a porous wall can be transformed so as to yield similar solutions in the transformed system, if the stream function f_W defining the flux through the wall does not vary. The transformed normal coordinate is

$$\eta = y(\rho_W U_\infty/\mu_W x)^{1/2}$$

and the transformed stream function is

$$f_W = \rho_W \psi/(\mu_W x U_\infty \rho_W)^{1/2}$$

and $u\rho = \partial\psi/\partial y$. The coordinates x and y are parallel and normal to the wall, respectively. An analogous solution for axisymmetric flow is presented in reference 9. Making use of the following (Mangler and Howarth) transformations for the case of stagnation flow

$$\gamma = \int_0^x \rho_W \mu_W \frac{du}{dx} x^3 \, dx \tag{A1}$$

$$\eta = \frac{(du/dx)\rho_e x^2}{\sqrt{2\gamma}} \int_0^y \frac{\rho}{\rho_e} \, dy \tag{A2}$$

in which the velocity at the boundary-layer outer edge (inviscid flow) is written

$$u_e = x \frac{du}{dx}$$

$$= B \frac{U_\infty}{R_N} x \tag{A3}$$

where B is a constant and R_N is the nose radius. A similarity parameter P_s can be obtained if equation (A2) is written in the inverted form

$$\frac{y}{R} = \frac{\sqrt{2\gamma}}{R(du/dx)x^2\rho_e} \int_o^\eta \frac{\rho_e}{\rho} \, d\eta \tag{A4}$$

Defining P_s as the coefficient of the integral and substituting equation (A3) yields

$$P_s = \frac{\sqrt{2}R}{BU_\infty x^2 \rho_e} \left(\int_o^x \rho_W \mu_W \frac{BU_\infty}{R} x^3 \, dx \right)^{1/2} = \frac{1}{\sqrt{2}\rho_e} \left(\frac{\rho_W \mu_W}{BU_\infty R} \right)^{1/2} \tag{A5}$$

and P_s can be expressed in terms of Reynolds number based on wall conditions, $R_{eW} = \rho_W R U_\infty / \mu_W$. Using the equations of state at the edge and wall with $p_W = p_e$ gives

$$\rho_e = \frac{p_W}{Z_e \mathcal{R} T_e} \quad \text{and} \quad \rho_W = \frac{p_W}{Z_W \mathcal{R} T_W}$$

Then from equation (A5)

$$P_s = \frac{1}{\sqrt{2B}} \frac{1}{\sqrt{R_{eW}}} \frac{Z_e T_e}{Z_W T_W} \tag{A6}$$

Alternatively, equation (A5) can be written in terms of the stream conditions. The density at the wall is

$$\rho_W = \frac{p_\infty g(U_\infty)}{Z_W T_W}$$

and $p_e \propto p_\infty$. Since the wall temperature and U_∞ are assumed to be constant,

$$\rho_W = K_1 \frac{\rho_\infty T_\infty}{Z_W} \tag{A7}$$

Writing the edge density as

$$\rho_e = \frac{p_e}{Z_e \mathcal{R} T_e} = \frac{p_\infty g_1(U_\infty)}{Z_e T_e} = \frac{\rho_\infty T_\infty}{Z_e T_e} g_2(U_\infty)$$

and substituting this and ρ_W from equation (A7) in equation (A5), we have

$$\left.\begin{aligned} P_s &= \frac{1}{\sqrt{2B}} \frac{Z_e T_e}{\rho_\infty g_2(U_\infty)} \sqrt{\frac{K_1 \rho_\infty \mu_W}{U_\infty R Z_W T_\infty}} \\ P_s &= g_3(U_\infty, T_\infty) \frac{Z_e T_e}{\sqrt{Z_W}} \sqrt{\frac{\mu_W}{\rho_\infty R}} \end{aligned}\right\} \tag{A8}$$

If the effects of pressure on the compressibility, temperature, and viscosity are neglected, the similarity parameter from equation (A8) is

$$P_s = \frac{F(U_\infty, T_\infty)}{\sqrt{\rho_\infty R}} \tag{A9}$$

As in the case of two-dimensional flow, the condition for similarity of boundary-layer solutions in the axisymmetric case is again that the transformed stream function at the wall be constant. This stream function is

$$\begin{aligned} f_W &= -v_W \rho_W \left(\rho_W \mu_W \frac{du}{dx}\right)^{-1/2} \\ &= -v_W \rho_W \left(\frac{R}{U_\infty \rho_W \mu_W B}\right)^{1/2} \end{aligned} \tag{A10}$$

To show that this condition is satisfied, when the scale varies, we obtain an expression for f_W corresponding to the ablation-product flux. In the physical system, the flux is $v_W \rho_W = \dot{m}$, where $\dot{m}$ is the mass rate of ablation, in mass per second per unit area. A convenient expression for $\dot{m}$ (see, e.g., ref. 16) is

$$\dot{m} = \dot{q}/H_{eff} \tag{A11}$$

where H_{eff} is the effective heat of ablation, assumed to be a function of surface material and stream velocity, and $\dot{q}$ is the cold-wall convective heating with no mass injection. The assumption that the heating is entirely convective is appropriate for the velocities considered here, but for somewhat higher velocities, effects of radiative heating would also have to be included. Convective heating from a stagnation region may be obtained from the relation given in reference 17,

$$\dot{q} = K_2 U_\infty^3 (\rho_\infty / R)^{1/2} \tag{A12}$$

Equation (A11) may then be written

$$\dot{m} = v_W \rho_W = \sqrt{\rho_\infty / R}\, g_3(U_\infty) \tag{A13}$$

Expressing stream density as

$$\rho_\infty = p_\infty / \mathcal{R} T_\infty$$

and wall density

$$\rho_W = p_\infty g(U_\infty) / Z_W T_W$$

and substituting equation (A13) in equation (A10) gives

$$f_W = -\sqrt{\frac{p_\infty}{\mathcal{R} T_\infty}}\, g_3(U_\infty) \sqrt{\frac{R}{\mu_W U_\infty B} \frac{Z_W T_W}{p_\infty g_1(U_\infty)}}$$

$$= -g_4(U_\infty, T_\infty) \sqrt{\frac{Z_W T_W}{\mu_W}} \tag{A14}$$

When the effect of pressure on compressibility is assumed to be small and the viscosity to be independent of pressure, this relation shows that at constant velocity, the transformed stream function does not vary with body size or stream density, so that the condition for boundary-layer similarity is met.[1]

The viscous core of the wake is considered to be described initially as a laminar free-shear layer converging to a minimum diameter at a constricted neck located about one body diameter downstream. At the neck, increased turbulence is assumed to disturb the laminar temperature and velocity profiles such as those calculated in reference 19 so that temperature, pressure, and concentration of injected gas are approximately constant across the diameter. Reference 4 indicates that a laminar base flow with turbulence beginning at the neck is possible throughout a large range of stream conditions. On the basis of experiments described in reference 1, and the analysis in reference 19, in which conditions on the dividing streamline of the laminar base flow are calculated, the velocity of the flow in the wake core is assumed to be independent of scale.

The similarity parameter given by equation (A9) is now used with the assumptions listed above to estimate effects of scale on radiation. First, the effect of varying body size with free-stream properties held constant is considered, and then the effect of maintaining the product $R\rho_\infty$ constant

[1]This result is also shown in reference 18 for the special case of convective heating alone, as part of a more general analysis of heating at higher speeds, including the effects of radiative heating and reradiation from heat shields.

(i.e., constant Reynolds number) is calculated. The first approach results in a very simple relation for the scale effect on radiation, whereas the second approach involves a more extended analysis requiring an expression for radiative intensity as a function of gas properties and concentration.

Constant Density

Equation (A4) written with the derived expression for the parameter P_s (eq. (A9)) becomes

$$\frac{y}{R} = \frac{F(U_\infty)}{\sqrt{\rho_\infty R}} \int_0^\eta \frac{\rho_e}{\rho} \, d\eta \tag{A15}$$

When the stream velocity and temperature are constant, it is apparent the boundary layer before separating has a thickness inversely proportional to the square root of the free-stream Reynolds number, which is also the classical result for nonablating surfaces.

The total mass flow in the boundary layer (where the subscript b refers to the boundary-layer edge at point of separation from the body surface) is expressed as

$$\dot{M}_B = 2\pi R^2 \rho_b U_b \int_0^{\delta/R} \frac{u\rho}{U_b \rho_b} \, d\left(\frac{y}{R}\right)$$

where $\delta = y$ at the point where $u\rho \approx U_b \rho_b$. If the similarity parameter P_s from equation (A9) is introduced and I_b represents the constant transformed integral,

$$\dot{M}_B = K_3 R^2 \rho_b U_b P_s I_b = K_4 \rho_b U_b \frac{R^{3/2}}{\sqrt{\rho_\infty}} I_b \tag{A16}$$

Since the wake core is considered to be composed of the boundary-layer flow (i.e., the entrainment of air due to mixing in the separated boundary layer just behind the body is neglected), the mass flow in the wake is equated to the boundary-layer flow

$$\dot{M}_w = A_w \rho_w U_w = \dot{M}_B \tag{A17}$$

where the subscript w refers to conditions representing the viscous wake at the station at which radiation effects are being studied.

The mass of ablation material contained in the wake can be calculated from the ablation rate (eq. (A13)) and the effective ablation area A_p, which is proportional to R^2. The rate of ablation is

$$\dot{M}_p = A_p \dot{m}$$

$$= K_5 R^2 \sqrt{\frac{\rho_\infty}{R}}\, g_3(U_\infty) \tag{A18}$$

Comparing this with equation (A16), one can see that for constant velocity U_∞ and constant stream density ρ_∞, both the total mass flux and the mass of ablated material vary with $R^{3/2}$. Thus the relative amounts of ablation material and of air remain constant as R varies. The mass of these components contained in a length l of the viscous wake can be computed as

$$\frac{M}{l} = \frac{\dot{M}}{U_W} \tag{A19}$$

in which U_W is an average wake-flow velocity relative to the body.

With equation (A17), a cross-section area and radius of the wake can be calculated:

$$A_W = \pi R_W^2 = \frac{\dot{M}_B}{\rho_W U_W} \tag{A20}$$

If we substitute $\dot{M}_B$ from equation (A16) and solve for R_W

$$R_W = K_6 \left(\frac{\rho_b U_b}{\rho_W U_W} \frac{R^{3/2}}{\sqrt{\rho_\infty}} I_b \right)^{1/2} \tag{A21}$$

It is assumed that the pressures p_b at the body base and p_W in the wake are constant fractions of the stream pressure. Then

$$\rho_b = \frac{p_b}{Z_b \mathcal{R} T_b} \propto \frac{p_\infty}{Z_b T_b} \tag{A22}$$

and

$$\rho_W = \frac{p_W}{Z_W \mathcal{R} T_W} \propto \frac{p_\infty}{Z_W T_W} \tag{A23}$$

In these expressions U_b, T_b, and Z_b are determined by the inviscid flow and do not vary with scale. As mentioned earlier, the wake velocity is relatively independent of scale. Equation (A12) then is

$$R_W = K_7 \left(Z_W T_W R^{3/2} \right)^{1/2} \tag{A24}$$

The wake temperature T_W varies to some extent as a result of variations in

the flow deflection at the base of the body and at the recompression shock wake; however, estimates indicate that the variation behind the trailing shock is not large. If it is assumed that this variation and the variation in Z_w can be neglected, equation (A24) reduces to

$$\frac{R_w}{R} = K_8 R^{-1/4} \tag{A25}$$

This analysis indicates that a variation in scale at constant-stream density and velocity produces no variation in the absolute densities of the two constituent gases, but a variation in wake radius given by equation (A25). On the supposition that the radiative intensity is determined by the concentration of the injected gas and the local properties of the mixture, the radiation from a fixed volume (watts/cm^3) is independent of scale. A possible restriction on the use of this result arises because of the assumption that the wake is optically thin. Among the materials studied, those producing bright wakes may be well represented by this assumption only at the lower densities and smaller scale factors.

Constant Reynolds Number

The effect on the peak radiative intensity of varying scale while maintaining constant Reynolds number (based on free-stream conditions) is investigated in this section. Constant Reynolds number here is meant to express $\rho_\infty R$ = constant. Equation (A21) can be written

$$\frac{R_w}{R} = \sqrt{\frac{\rho_b U_b}{\rho_w U_w}} (Re_\infty)^{-1/4} (I_b)^{1/2} \tag{A26}$$

As before, using the assumption that the velocities U_b and U_w are constant fractions of U_∞, and inserting equations (A22) and (A23) in equation (A26) gives

$$\frac{R_w}{R} = K_8 \sqrt{\frac{Z_w T_w}{Z_b T_b}} (Re_\infty)^{-1/4} (I_b)^{1/2} \tag{A27}$$

In the approximate analysis presented here, it is consistent to assume again that variations in temperature and compressibility ratios can be neglected. Then

$$\frac{R_w}{R} = K_9 (Re_\infty)^{-1/4} \tag{A28}$$

The variation of wake radius given by equation (A28) has been compared with that obtained from the tests. The experimental results shown in figure 16 were obtained by measuring the width of the luminous wake recorded with image converter and Kerr-cell camera photographs. The one-fourth power variation is in agreement with the measurements.

For scale variations with the product $\rho_\infty R$ constant, the flow geometry and transition characteristics are unchanged. Also, from the boundary-layer similarity conclusions, the ablation gas concentration does not vary. This is shown by the ratio $\dot{M}_P/\dot{M}_B$ where $\dot{M}_B$ is given by equation (A16) and $\dot{M}_P$ is obtained from equation (A18). The mass ratio then is

$$\frac{\dot{M}_P}{\dot{M}_B} = K_{10} \frac{\rho_\infty g_2(U_\infty)}{\rho_b U_b I_b} \propto Z_b T_b \tag{A29}$$

If the effects of scale on the temperature and compressibility are again assumed to be negligible, this ratio is a constant.

Radiant intensity equation.- With $\rho_\infty R$ constant, changes in scale lead to inverse changes in density. Thus, an expression is needed to relate observed radiant intensity to that at conditions to which the scaling relations apply. The following relation was used in reference 8 to express radiative output from ablation products in a boundary layer. If I is the power per unit volume,

$$I/\rho_P = \Gamma \rho_w^{\zeta} T_w^{\xi} \text{ , watts/g} \tag{A30}$$

where ρ_P is the density of injected ablation gas, ρ_w is the total gas density, Γ is a constant, and ζ and ξ are exponents to be evaluated. Applying this formula to radiation per unit length of wake gives

$$A_w I = \Gamma A_w \rho_P \rho_w^{\zeta} T_w^{\xi} \text{ , watts/cm} \tag{A31}$$

Noting that $\rho_P = \dot{m} A_P / U_w A_w$ where A_P is the effective ablation area, equation (A13) furnishes a relation for the ablation gas density

$$\rho_P = K_{11} \frac{R^{3/2} \rho_\infty^{1/2} g_2(U_\infty)}{U_w A_w} \tag{A32}$$

Combining equations (A17) and (A16) gives the total density in the wake, ρ_w,

$$\rho_w = \frac{K_4}{A_w U_w} \rho_b U_b R^{3/2} \rho_\infty^{-1/2} I_b \tag{A33}$$

When the proportionalities $U_b \propto U_\infty$ and $\rho_b \propto \rho_\infty / Z_b T_b$ are inserted, equation (A31) is

$$A_w I = K R^{3/2} \rho_\infty^{1/2} \frac{g_2(U_\infty)}{U_w} \left(\frac{R^{3/2} I_b \rho_\infty^{1/2} U_\infty}{A_w U_w Z_b T_b} \right)^{\zeta} T_w^{\xi} \tag{A34}$$

Making use of the previously listed assumptions (Z_b, T_b, U_∞ and U_w constant) in equation (A34), we have

$$A_w I = K_{12} R \sqrt{R\rho_\infty}\ \rho_\infty^{\zeta} T_\infty^{\xi} \tag{A35}$$

If the following is substituted for wake area (from eq. (A28))

$$A_w = \pi R_w^2 \propto \frac{R^2}{\sqrt{R\rho_\infty}} \tag{A36}$$

equation (A35) gives the following radiant power per unit volume.

$$I = \left(\frac{K_{13}\rho_\infty^{\zeta} T^{\xi}}{R}\right)\left(R\rho_\infty\right) \tag{A37}$$

Thus except for the nonzero exponent on ρ_∞ and the variation of temperature with density, the optical thickness is preserved if Reynolds number is held constant; that is, the emissive power is inversely proportional to the scale factor. If the test velocity is adjusted to hold temperature constant and minor adjustments of density are made to preserve Reynolds number, better simulation of large-scale bodies might be achieved in the ballistic range.

If we insert the observed variation with density of radiant power per body diameter (let ξ take on the value 4 (ref. 8)) and include the variation of temperature with density calculated for equilibrium air at constant enthalpy, the following approximate expression is obtained:

$$I = K_{14} R^{-3/2} \tag{A38}$$

or

$$W = 2\pi R_w^2 R I \propto \frac{I R^3}{\sqrt{R_e}} \tag{A39}$$

$$W = K_{15} R^{3/2} \tag{A40}$$

This furnishes a relation for scaling the radiant power from a length of wake equal to the body diameter at constant Reynolds number.

REFERENCES

1. Hidalgo, Henry; Taylor, R. L.; and Keck, J. C.: Transition in the Viscous Wakes of Blunt Bodies Flying at Hypersonic Speeds. J. Aerospace Sci., vol. 29, no. 11, Nov. 1962, pp. 1306-1315, 1331.

2. Bradford, W. H.; and Siperly, B. H.: Methods of Analysis of Microwave Scattering From Wakes of Hypervelocity Projectiles. AE62-0218M, Space Sci. Lab., General Dynamics/Astronautics, Feb. 1962.

3. Feldman, Saul: On Trails of Axisymmetric Hypersonic Blunt Bodies Flying Through the Atmosphere. J. Aerospace Sci., vol. 28, no. 6, June 1961, pp. 433-48, 470.

4. Lees, Lester; and Hromas, Leslie: Turbulent Diffusion in the Wake of a Blunt-Nosed Body at Hypersonic Speeds. J. Aerospace Sci., vol. 29, no. 8, Aug. 1962, pp. 976-993.

5. Goulard, Madeleine; and Goulard, Robert: The Aerothermodynamics of Reentry Trails. ARS Semiannual Meeting, May 9-12, 1960.

6. Page, William A.; and Arnold, James O.: Shock-Layer Radiation of Blunt Bodies at Reentry Velocities. NASA TR R-193, 1964.

7. Compton, Dale L.; and Cooper, David M.: Measurements of Radiative Heating on Sharp Cones. AIAA paper 64-252.

8. Craig, Roger A.; and Davy, William C.: Thermal Radiation From Ablation Products Injected Into a Hypersonic Shock Layer. NASA TN D-1978, 1963.

9. Davy, William C.; Craig, Roger A.; Chapman, Gary T.; and Compton, Dale L.: Ablation Product Radiation From Cones. AIAA paper 64-71.

10. Seiff, Alvin: Ames Hypervelocity Free-Flight Research. Astronautics and Aerospace Engineering, vol. 1, no. 11, Dec. 1963, pp. 16-23.

11. Compton, Dale L.; and Chapman, Gary T.: Two New Free-Flight Methods for Obtaining Convective Heat-Transfer Data. Proc. AIAA Aerodynamic Testing Conference, Washington, D. C., Mar. 9-10, 1964, pp. 115-128.

12. Slattery, R. E.; and Clay, W. G.: Measurement of Turbulent Transition, Motion, Statistics and Gross Radial Growth Behind Hypervelocity Objects. Phys. Fluids, vol. 5, no. 7, July 1962, pp. 849-855.

13. Kivel, B.; and Bailey, K.: Tables of Radiation from High Temperature Air. Res. Rep. 21, Avco Res. Lab., Dec. 1957.

14. Page, William A.; Canning, Thomas N.; Craig, Roger A.; and Stephenson, Jack D.: Measurements of Thermal Radiation of Air From the Stagnation Region of Blunt Bodies Traveling at Velocities up to 31,000 Feet per Second. NASA TM X-508, 1961.

15. Brown, W. B.; and Livingood, John N. B.: Solutions of Laminar-Boundary-Layer Equations Which Result in Specific-Weight-Flow Profiles Locally Exceeding Free-Stream Values. NACA TN 2800, 1952.

16. Georgiev, Steven; Hidalgo, Henry; and Adams, Mac C.: On Ablating Heat Shields for Satellite Recovery. Res. Rep. 65, Avco-Everett Res. Lab., 1959.

17. Chapman, Dean R.: An Analysis of the Corridor and Guidance Requirements for Supercircular Entry into Planetary Atmospheres. NASA TR R-55, 1960.

18. Howe, John T.; and Sheaffer, Yvonne S.: Mass Addition in the Stagnation Region for Velocity up to 50,000 Feet per Second. NASA TR R-207, 1964.

19. Denison, M. Richard; and Baum, Eric: Compressible Free Shear Layer With Finite Initial Thickness. AIAA Jour., vol. 1, no. 2, Feb. 1963, pp. 342-349.

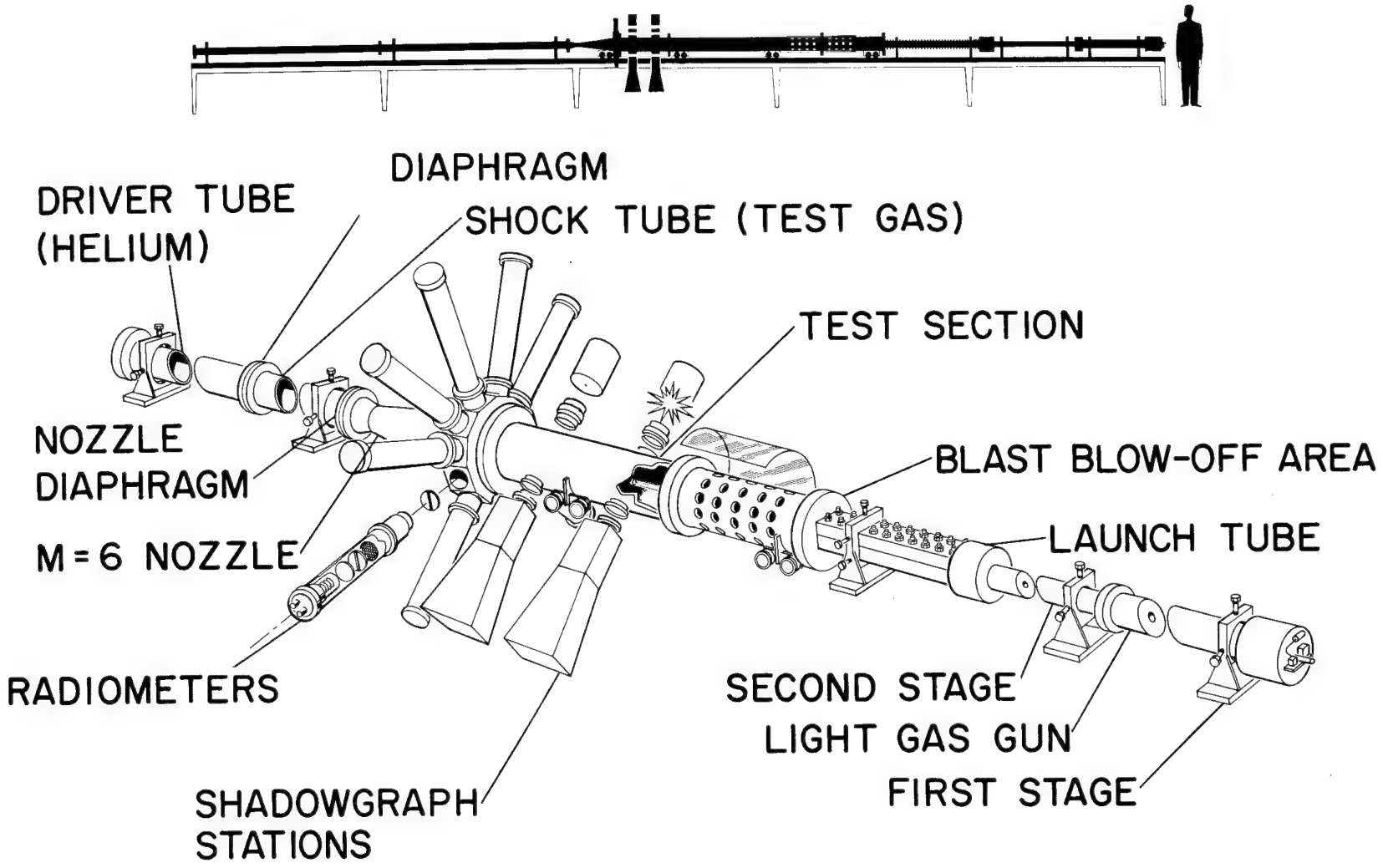

Figure 1.- Schematic drawing of pilot hypersonic free-flight facility.

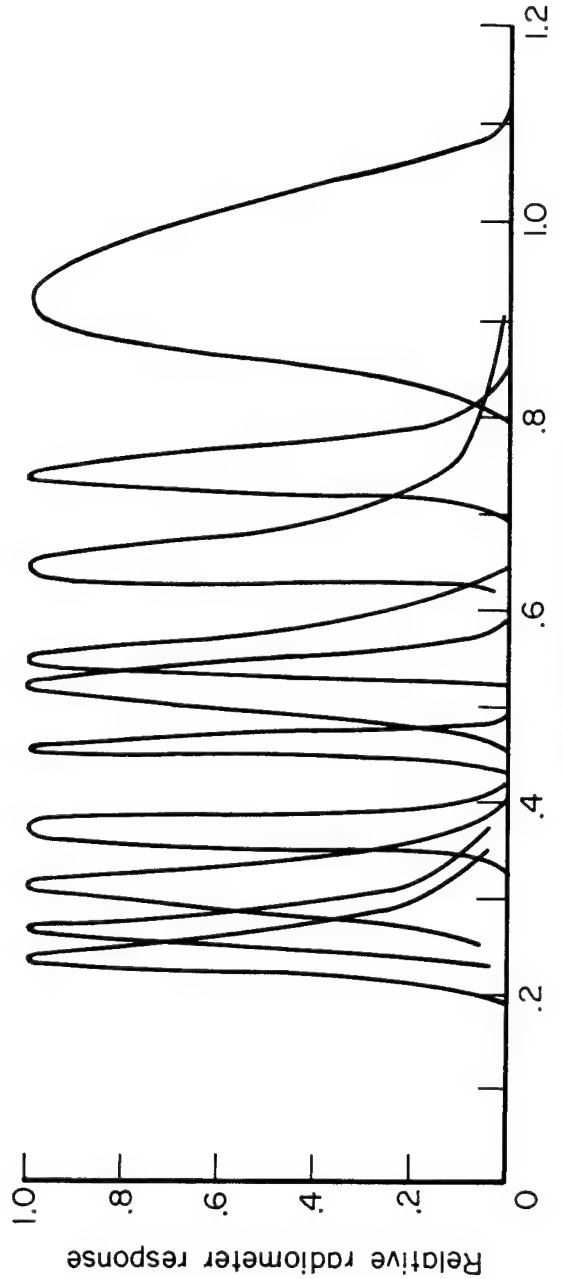

Figure 2.- Radiometer responses as functions of wavelength.

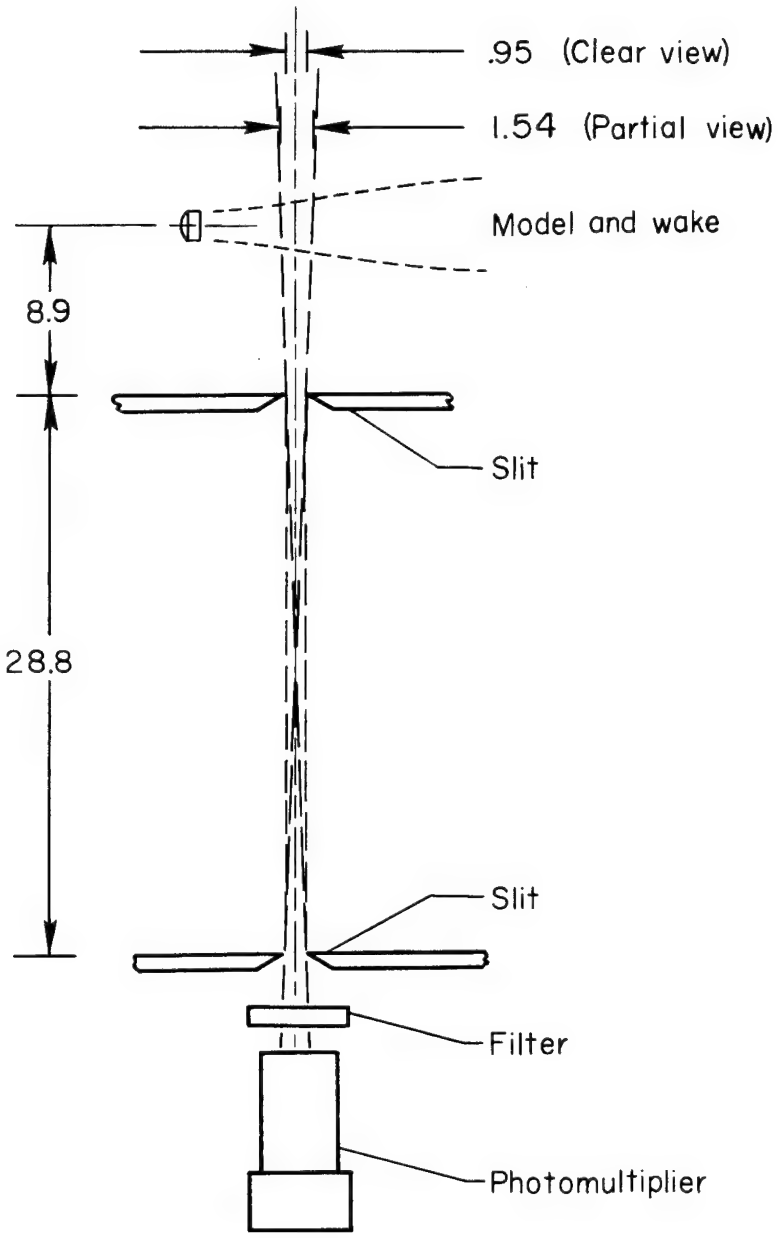

NOTE: Dimensions in cm

Figure 3.- Radiometer and slit arrangement.

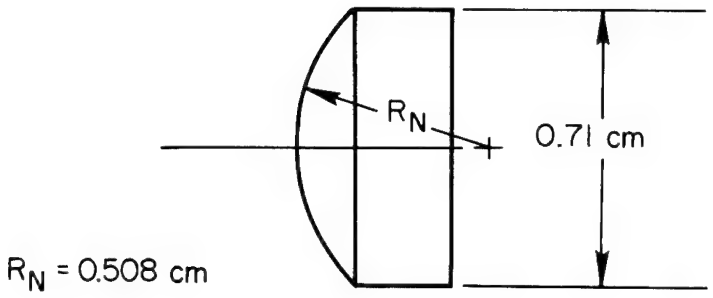

Standard model

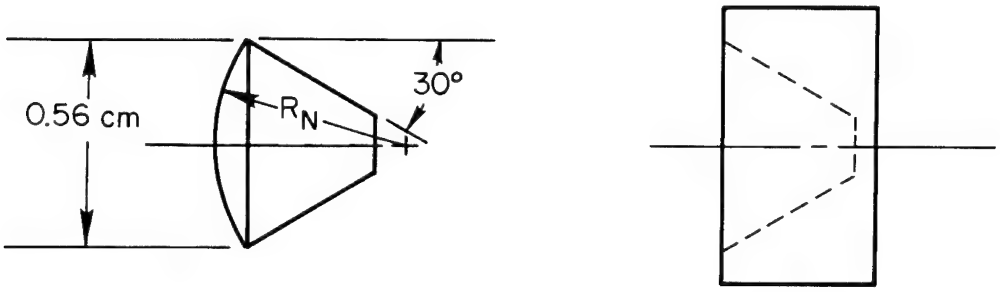

Sabot-launched model

Sabot

Figure 4.- Model geometry.

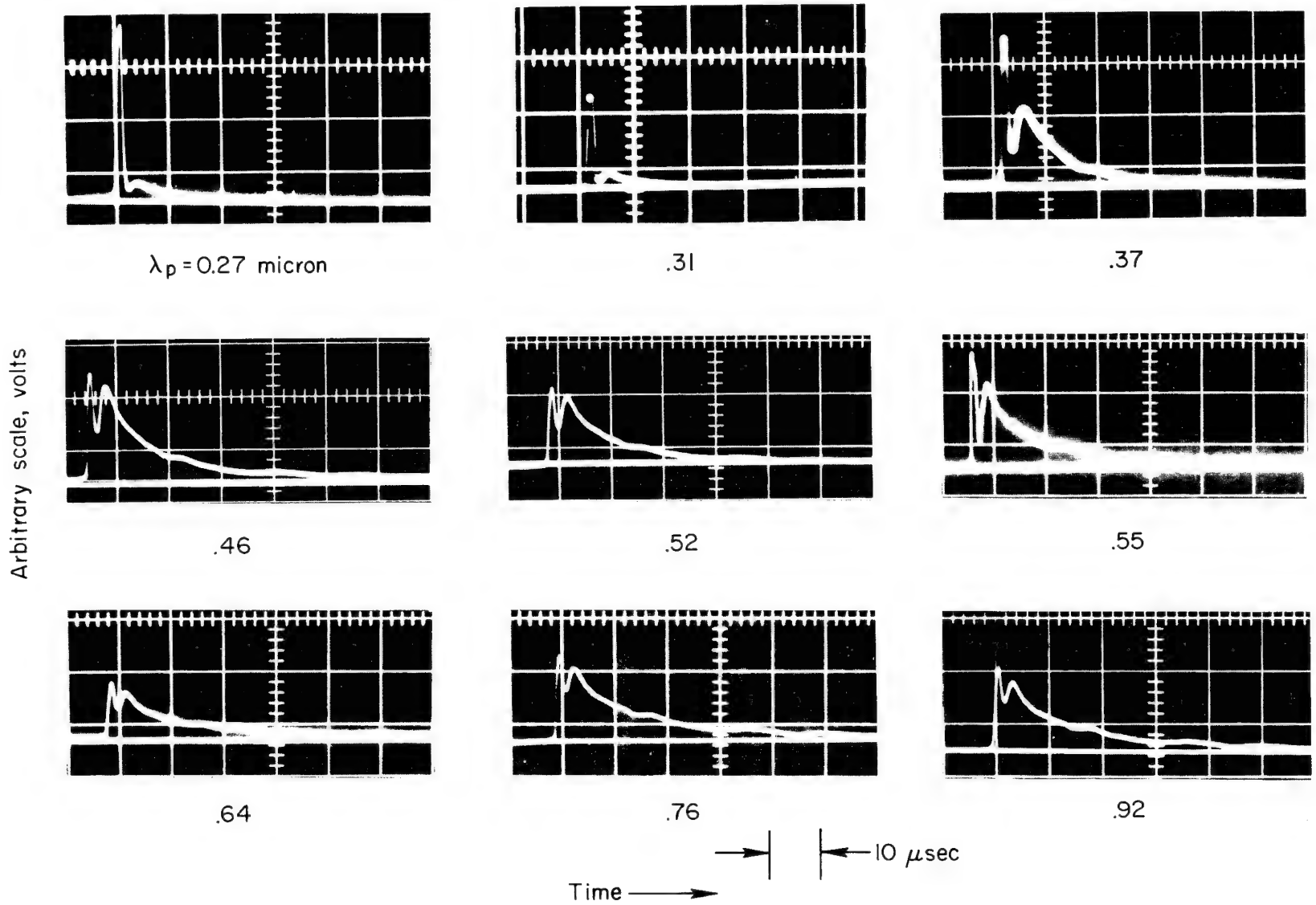

(a) Oscillograms showing radiometer output signals at a series of wavelengths; U_∞ = 6.6 km/sec, ρ_∞/ρ_o = 0.07, polycarbonate.

Figure 5.- Wake radiation data.

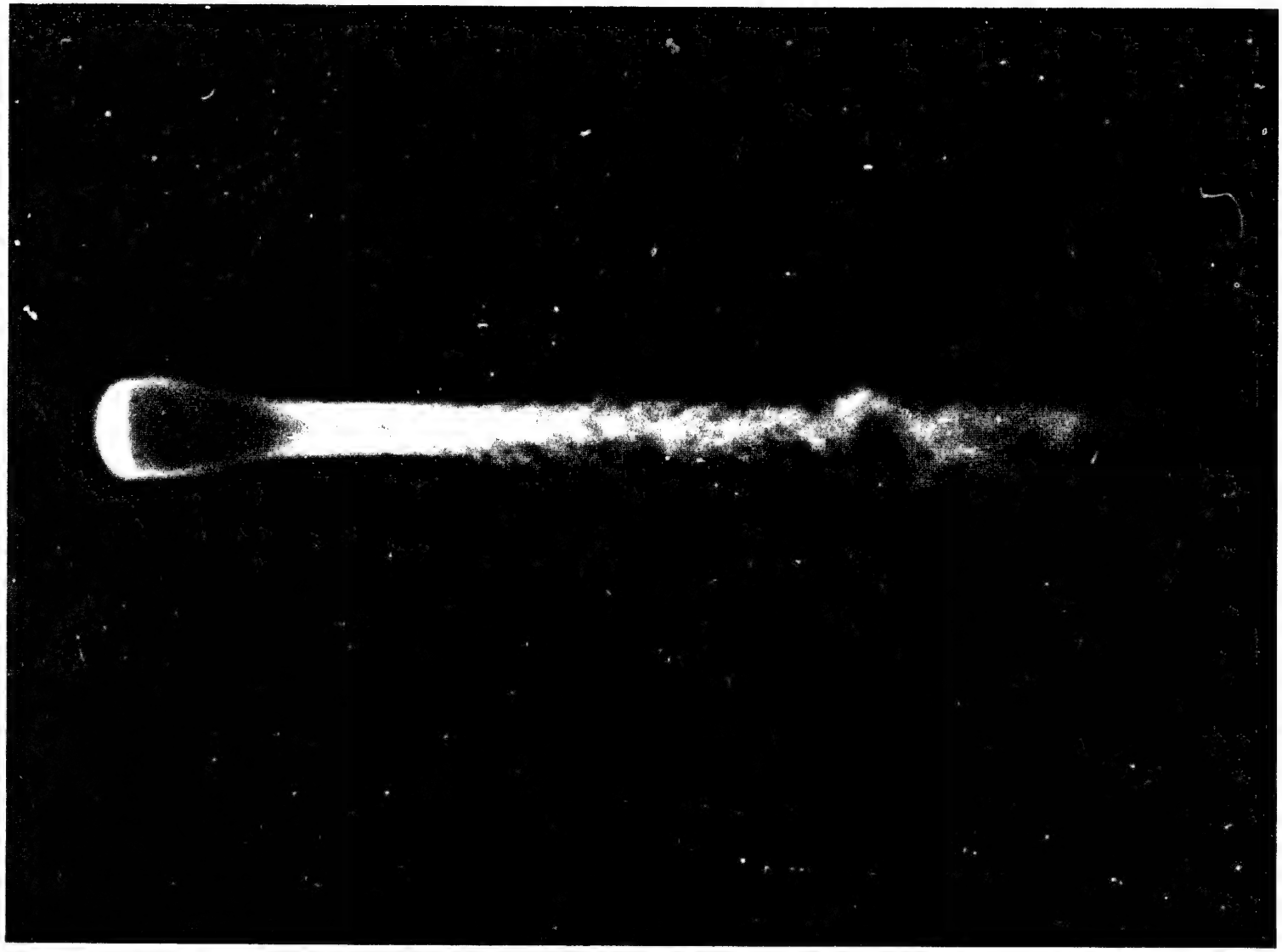

(b) Image converter photograph of luminous flow; polycarbonate model, U_∞ = 6.6 km/sec.

Figure 5.- Concluded.

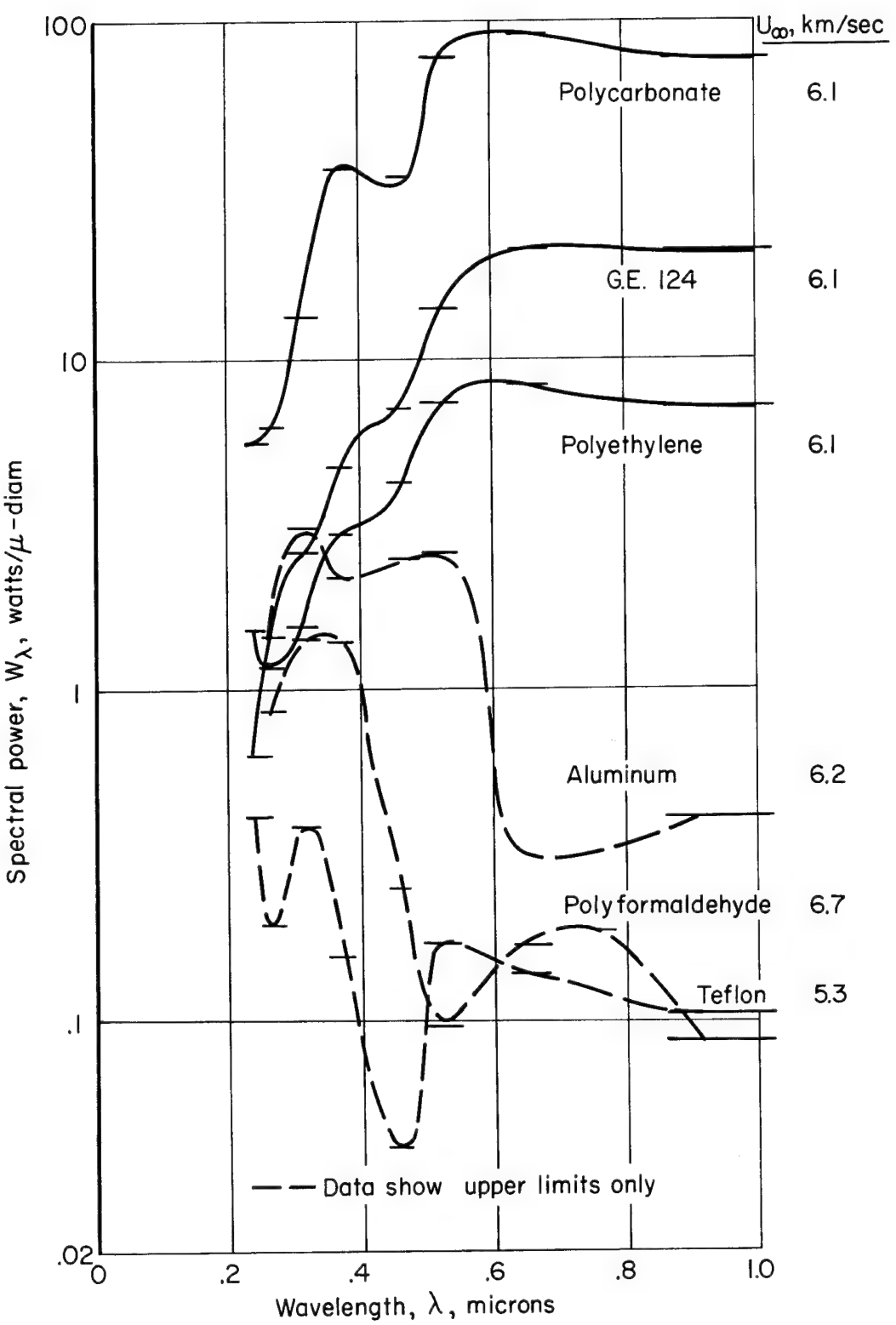

Figure 6.- Spectra of peak wake radiance for models made of various materials; ambient pressure, 60 mm Hg.

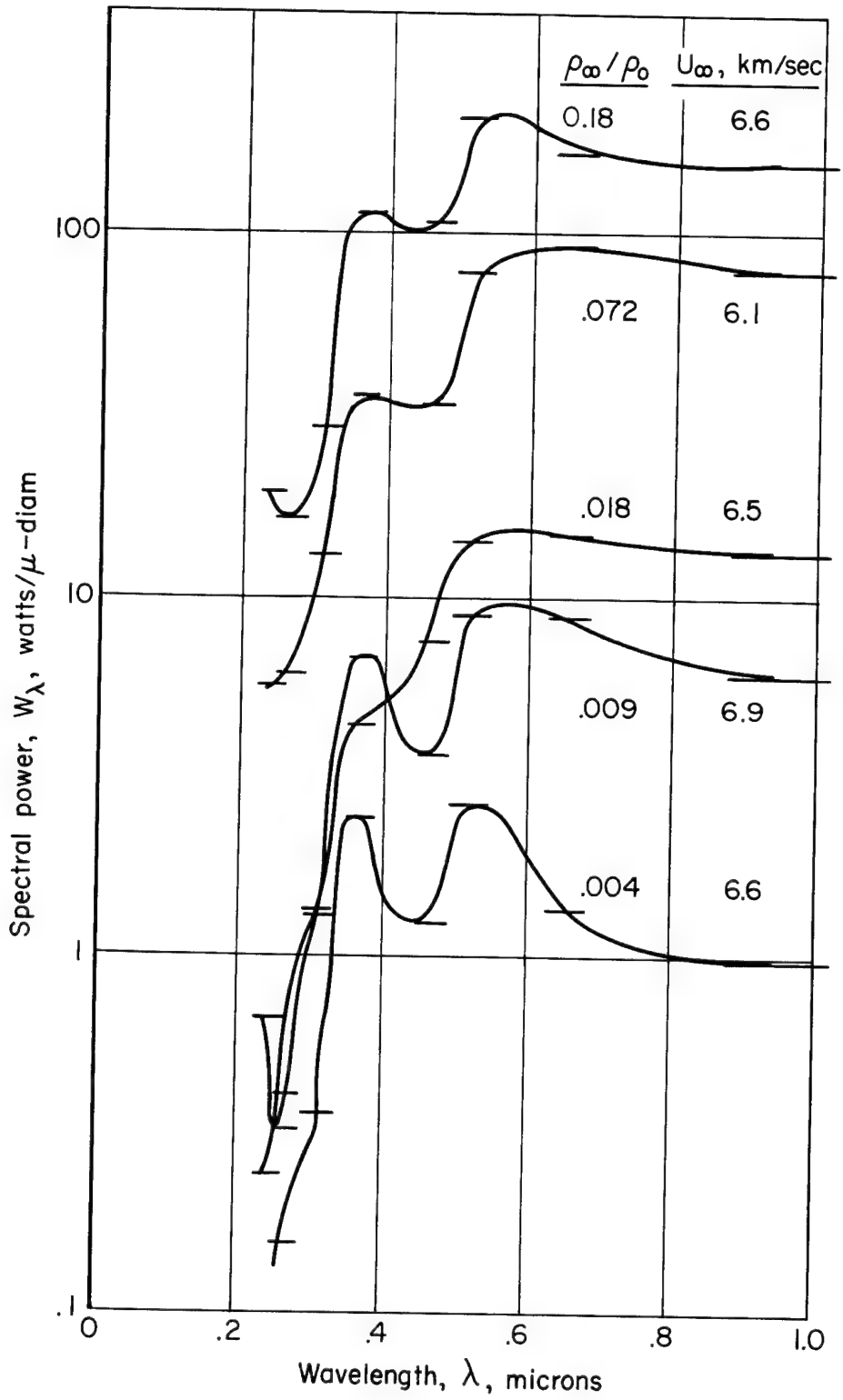

(a) Polycarbonate.

Figure 7.- Peak wake spectra at various stream densities.

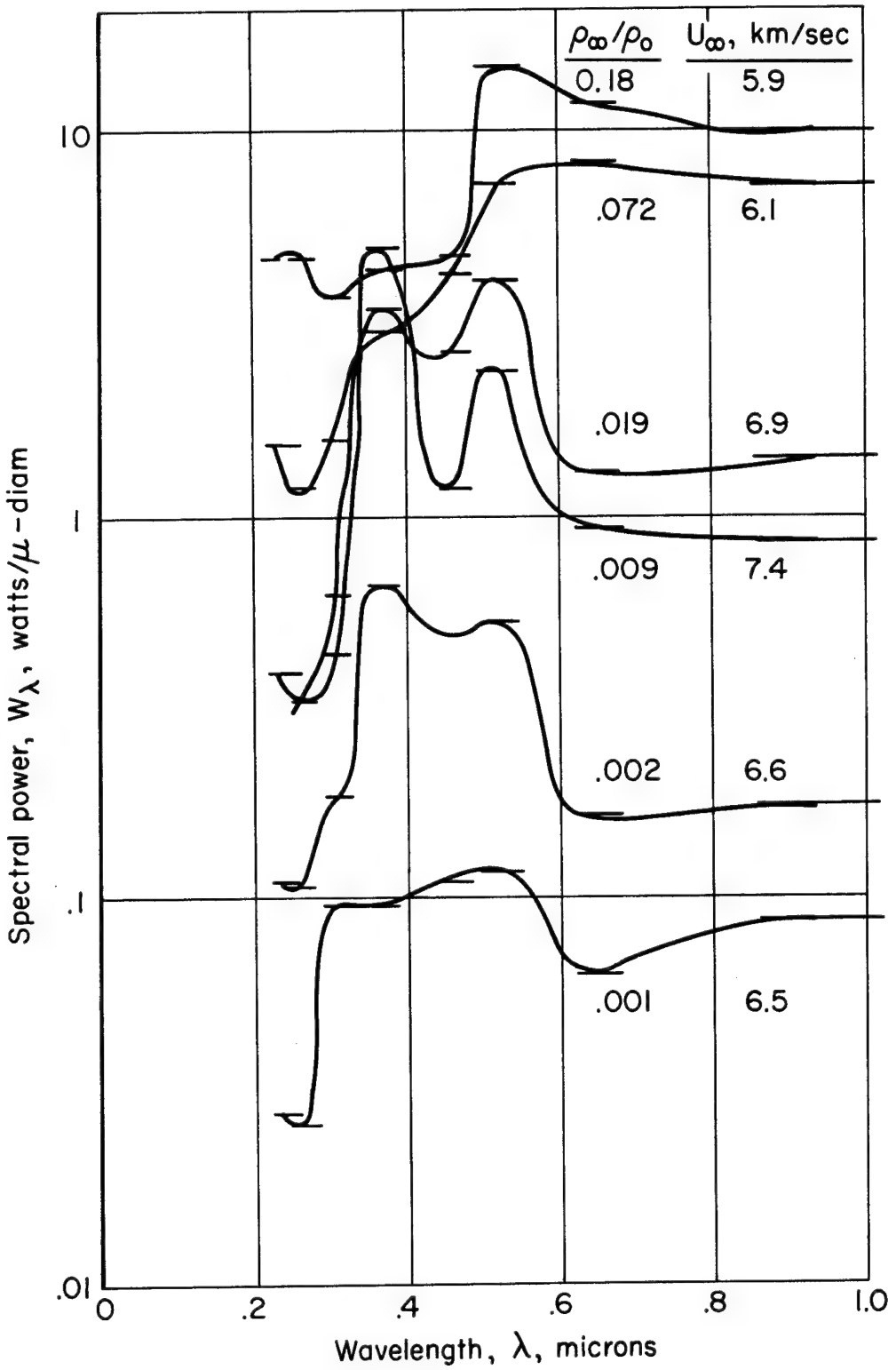

(b) Polyethylene.

Figure 7.- Concluded.

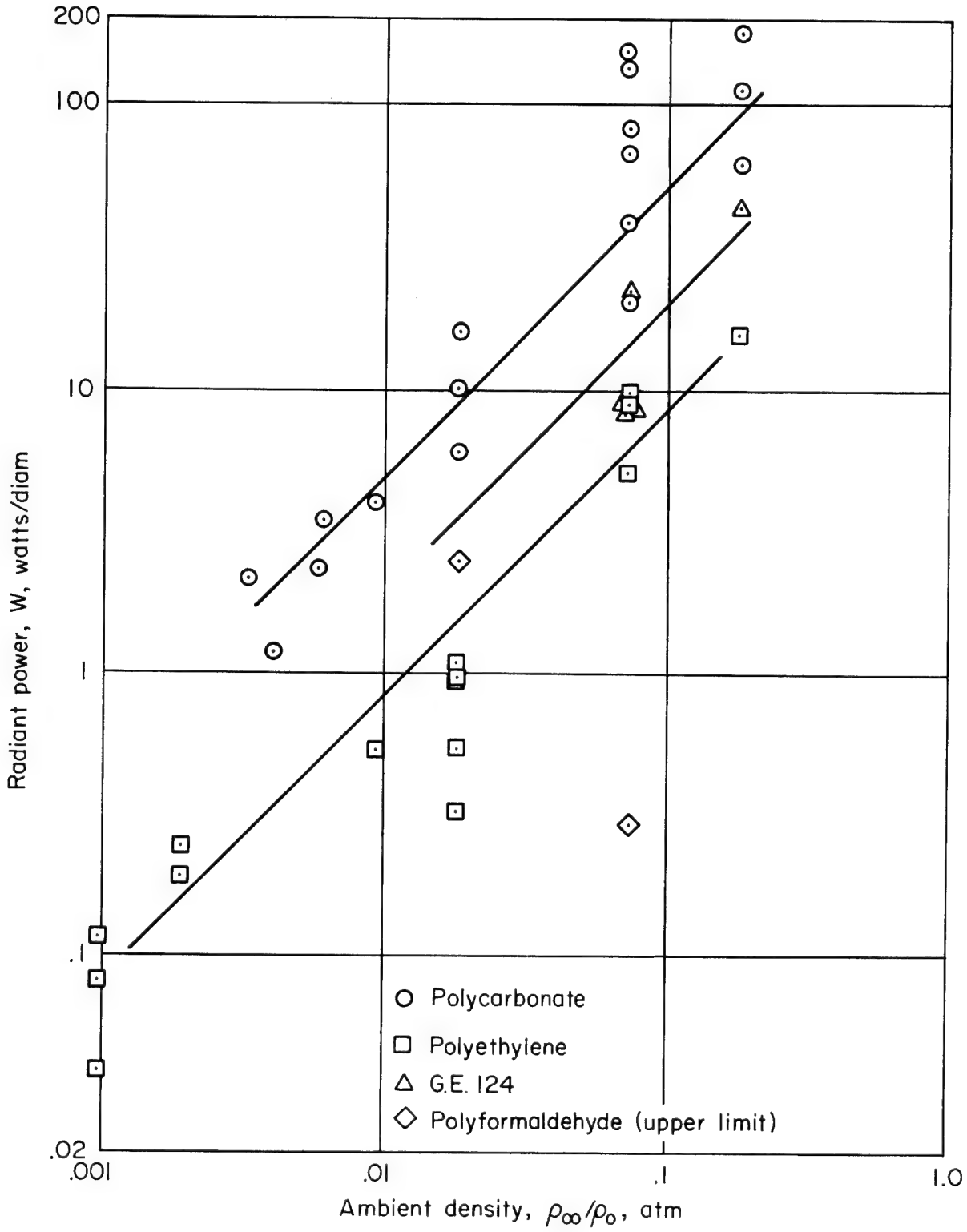

(a) U_∞ = 6.7 km/sec

Figure 8.- Measured radiative power (in spectral region from 0.2 to 1.0 μ) in wake at location of peak radiance as a function of stream density.

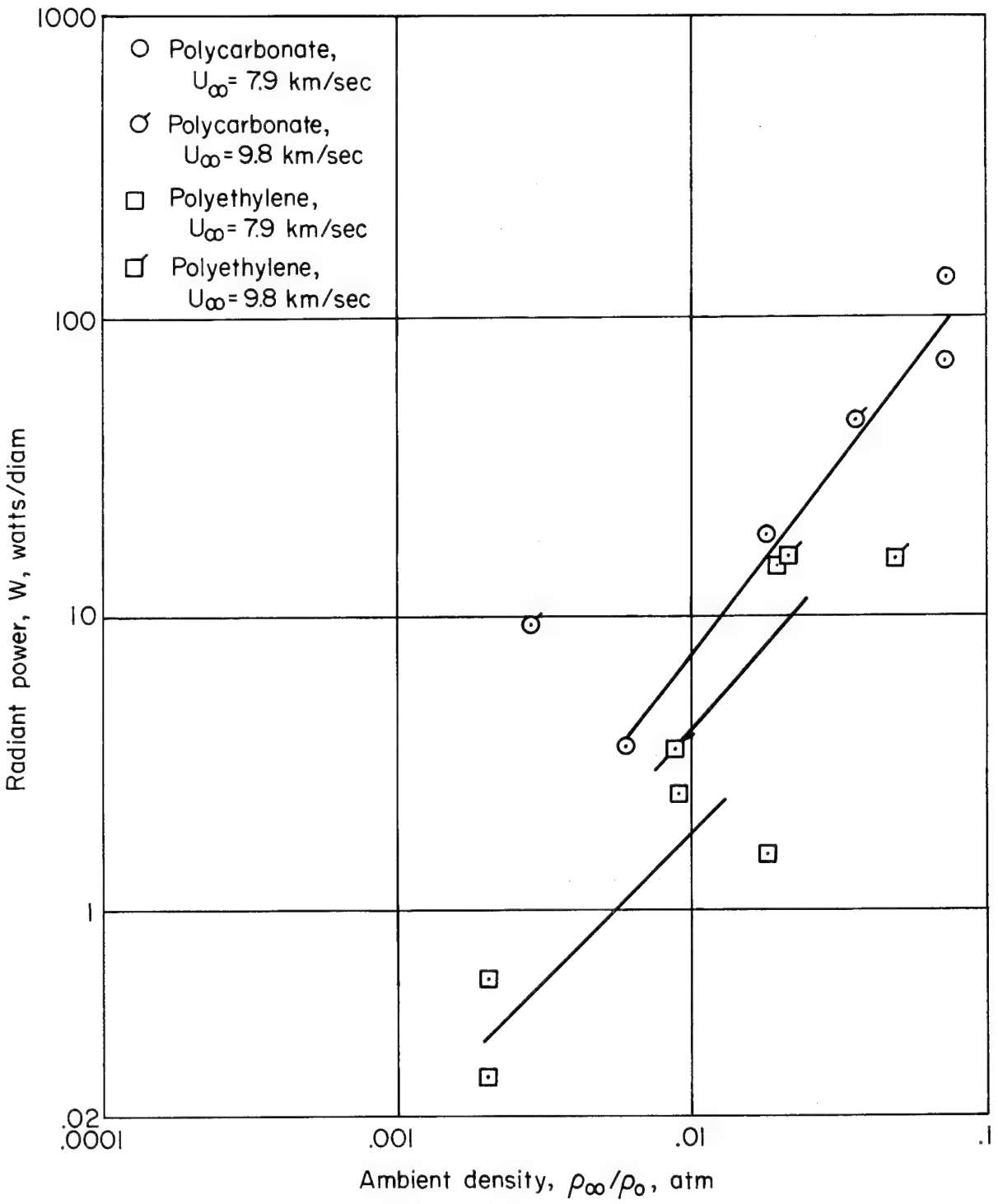

(b) U_∞ = 7.9 and 9.8 km/sec

Figure 8.- Concluded.

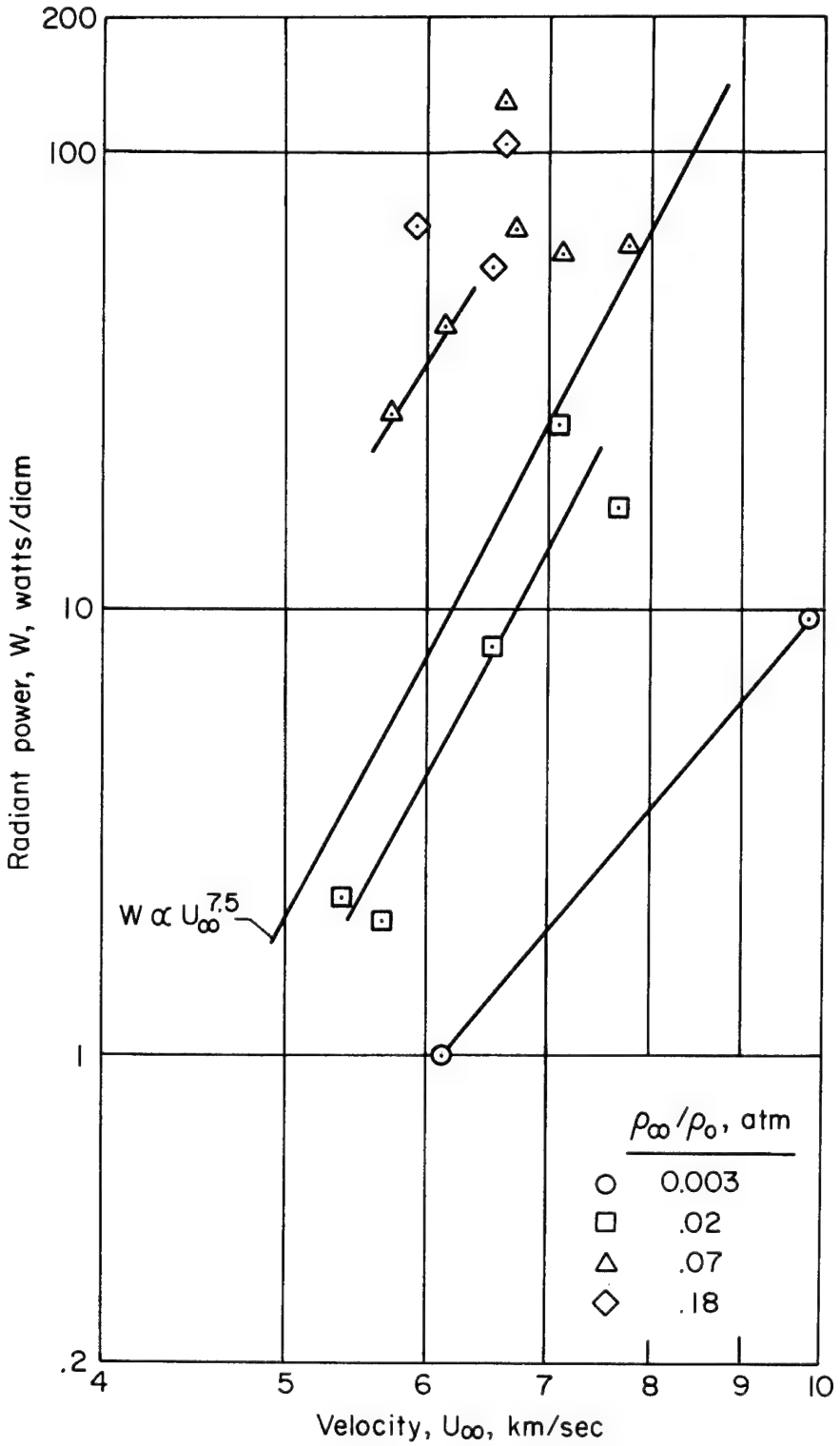

(a) Polycarbonate.

Figure 9.- Effect of model velocity on the measured peak radiative power of the wake.

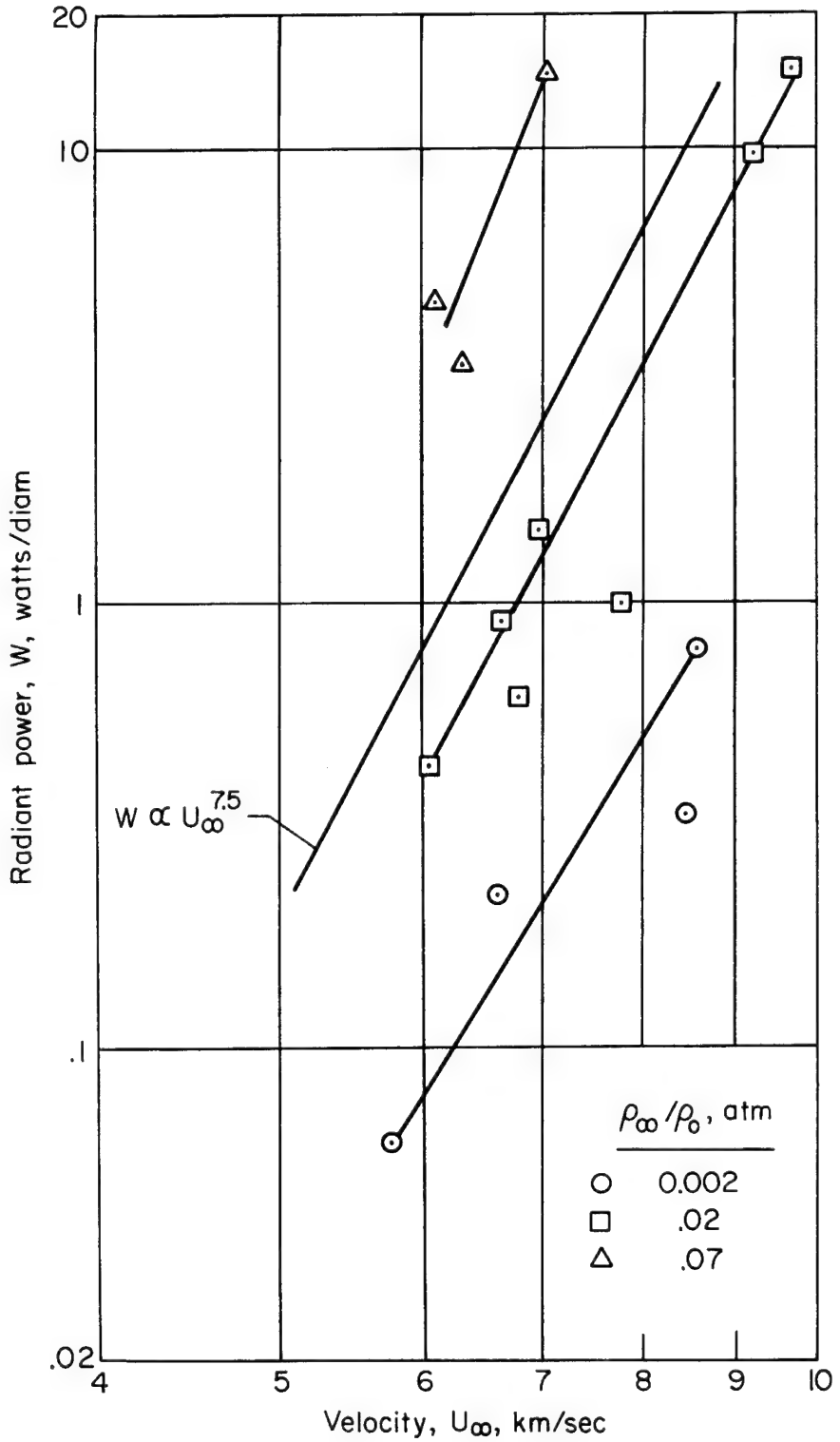

(b) Polyethylene.

Figure 9.- Concluded.

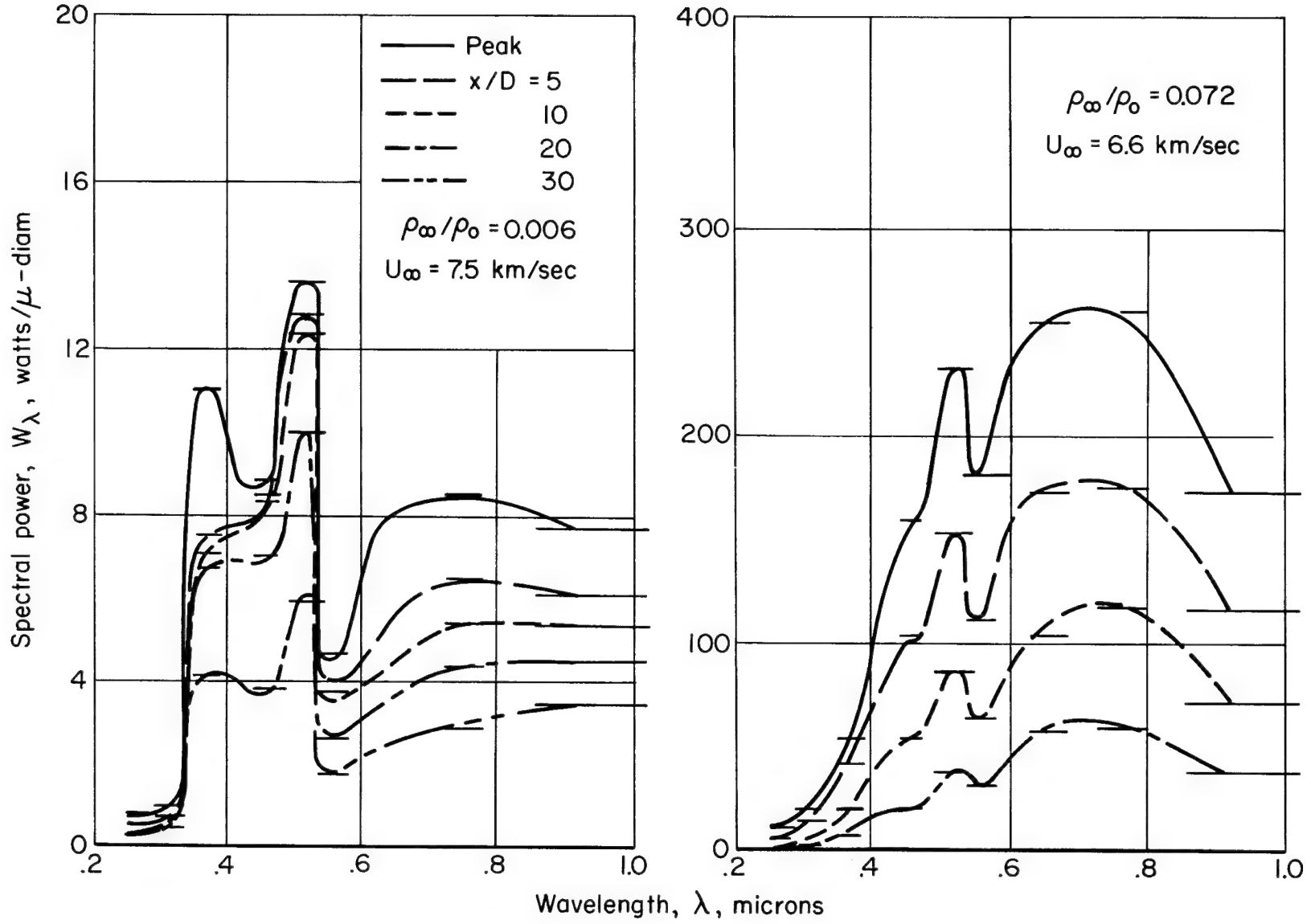

(a) Polycarbonate.

Figure 10.- Wake spectra at various longitudinal locations behind model.

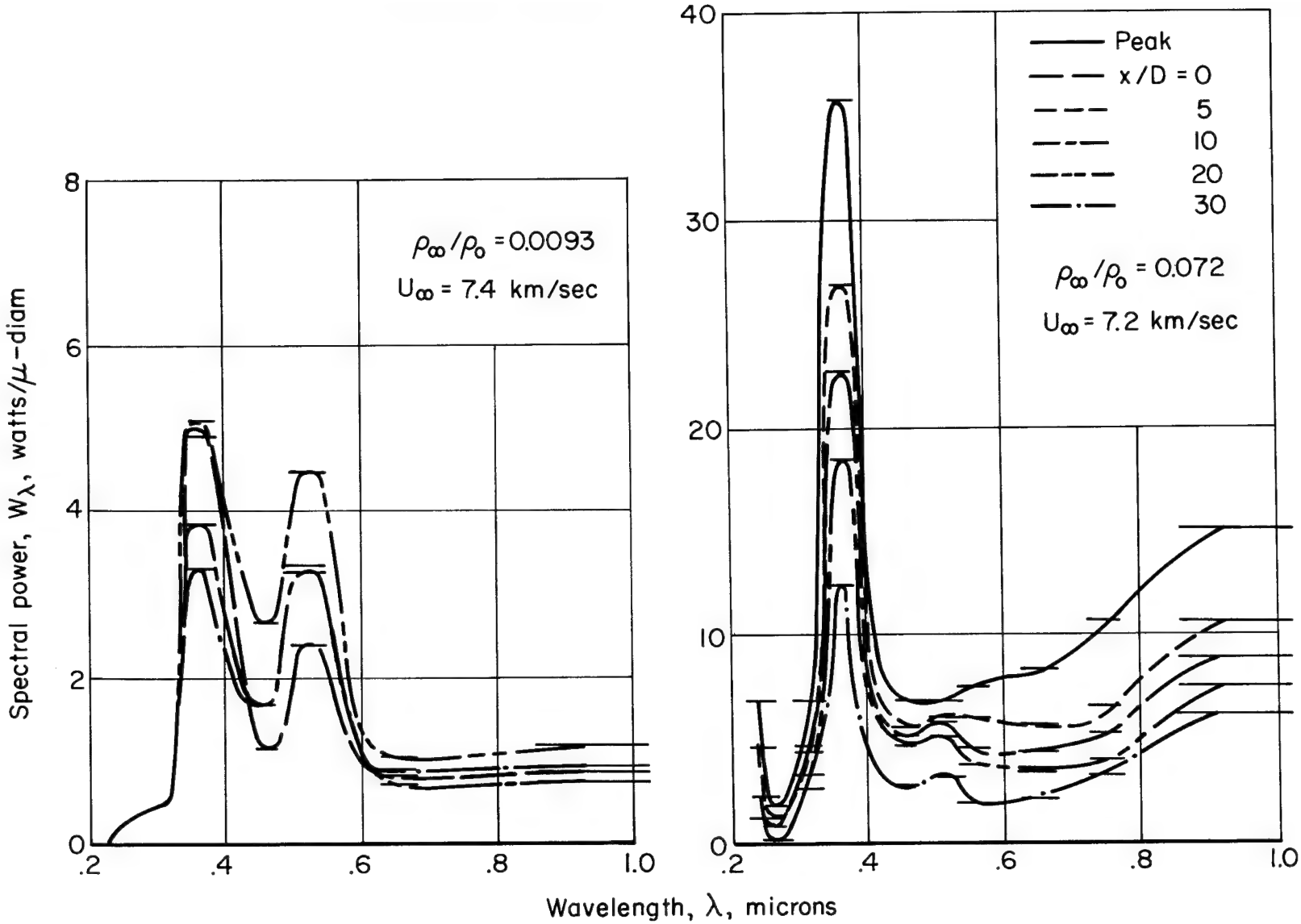

(b) Polyethylene.

Figure 10.- Continued.

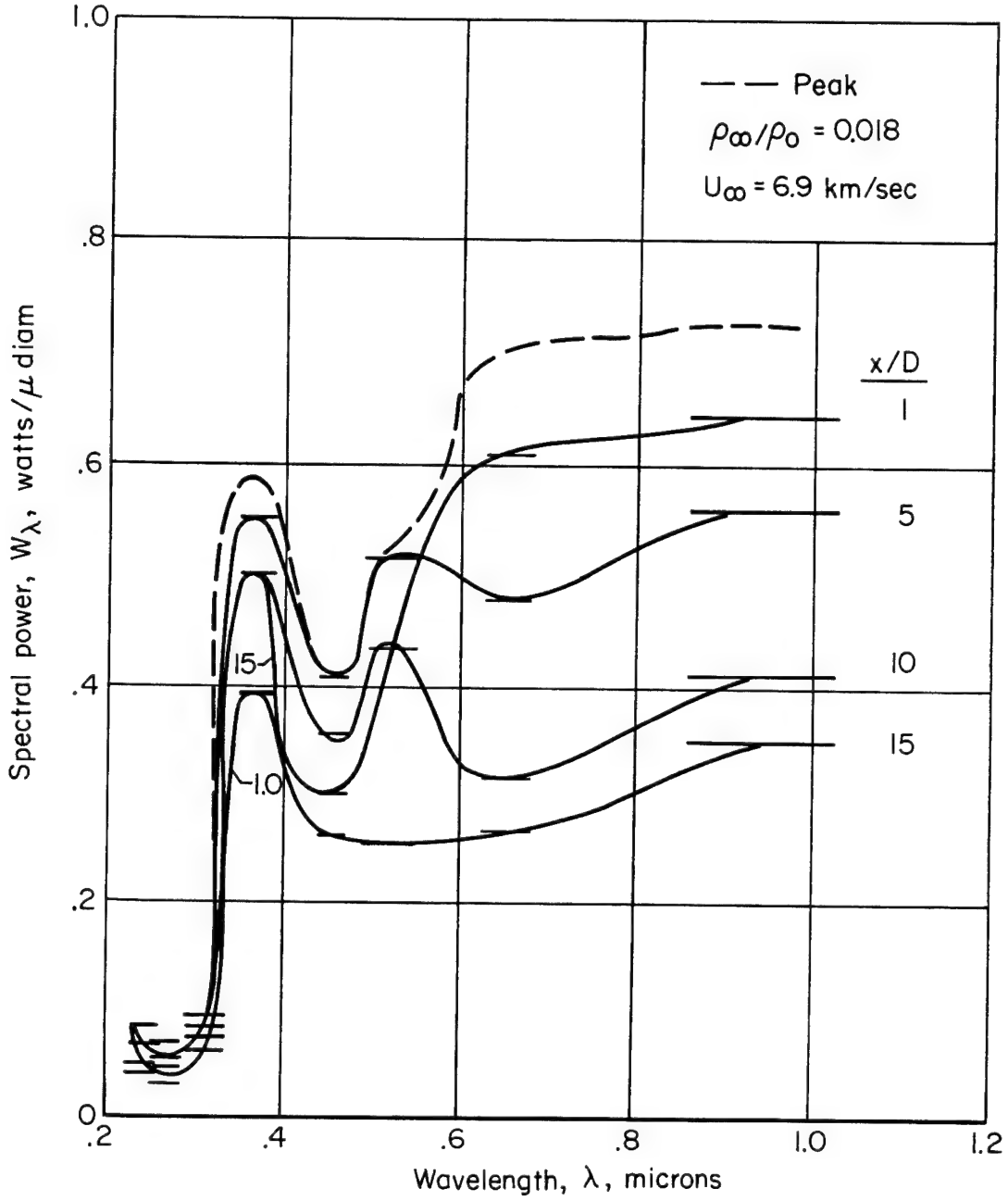

(c) G. E. 124.

Figure 10.- Concluded.

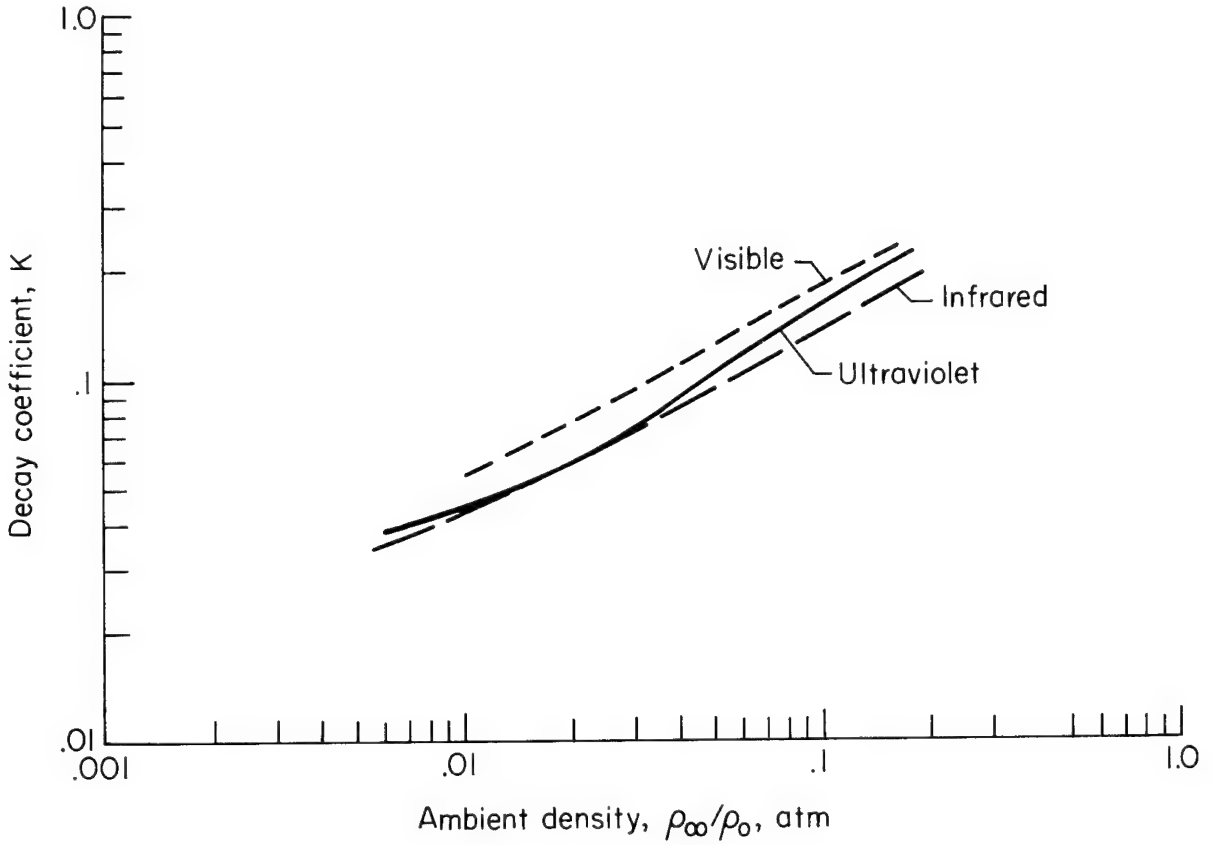

Figure 11.- Decay rate of wake luminosity for polycarbonate and G. E. 124 models; U_∞ = 5.9 to 8.2 km/sec.

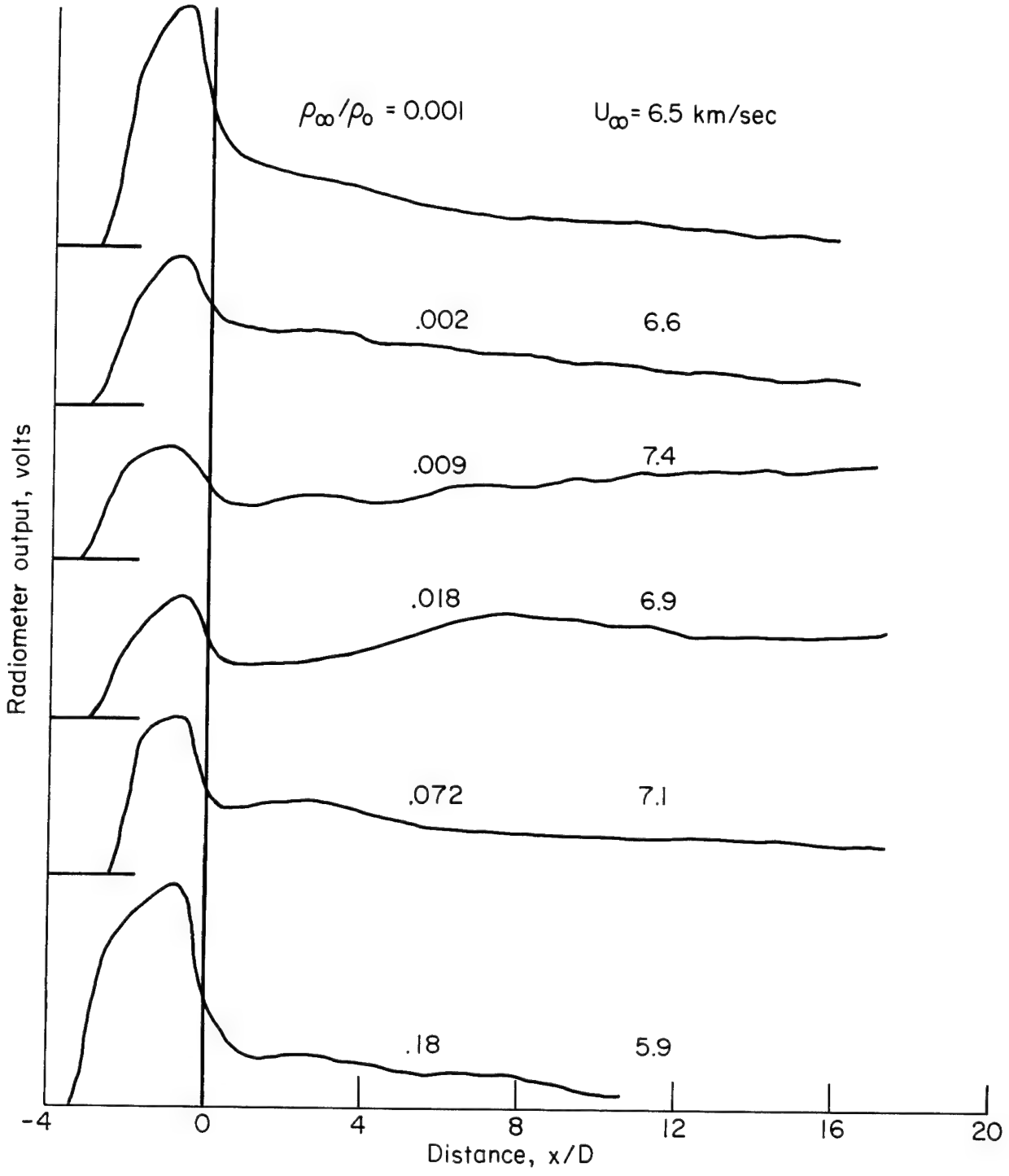

Figure 12.- Longitudinal distribution of wake luminosity in the wavelength region 0.45 to 0.59 micron for polyethylene models.

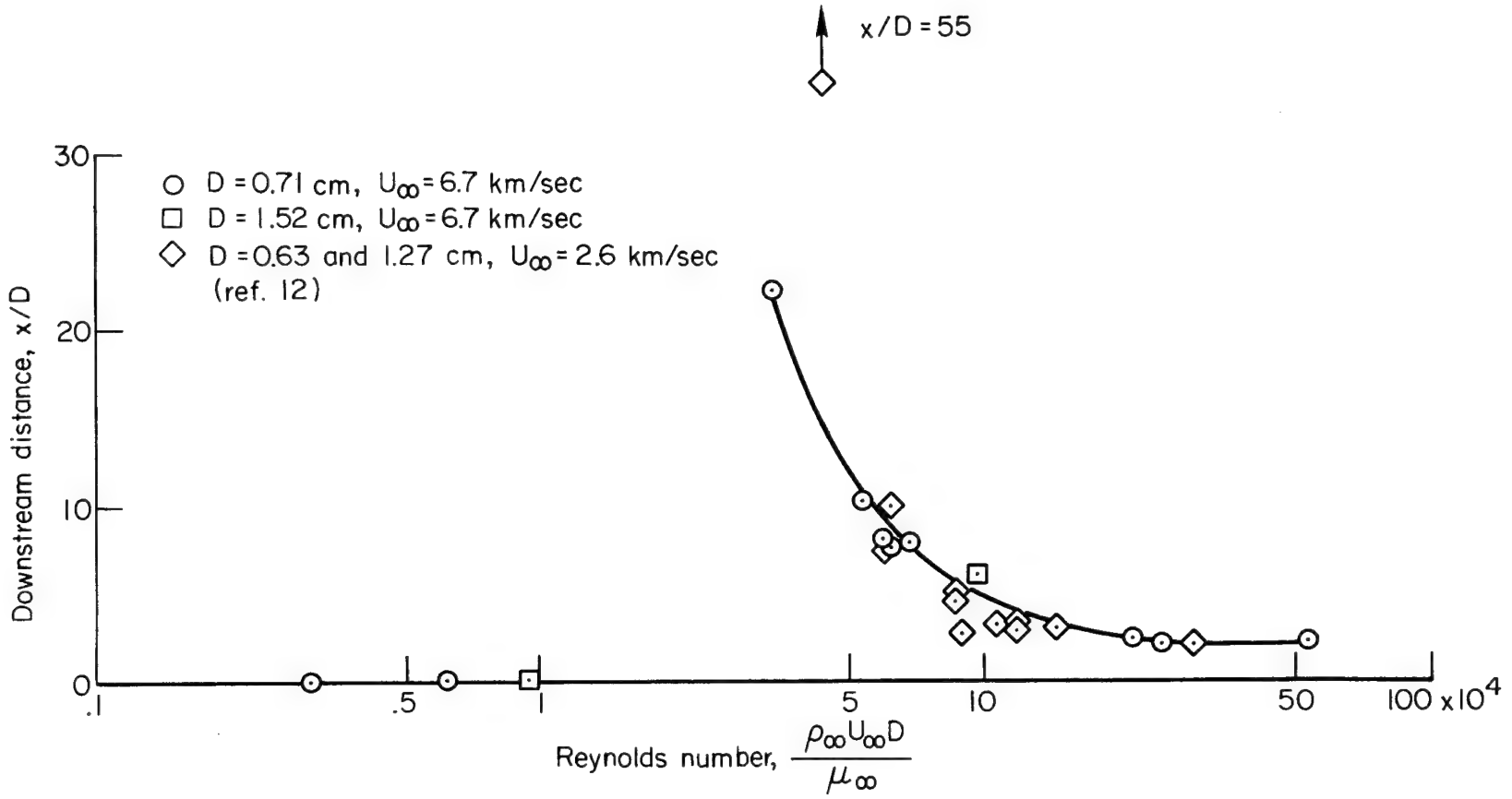

Figure 13.- Longitudinal location of peak luminosity in polyethylene model wakes in the wavelength band 0.45 to 0.59 micron and comparison with wake transition measurements.

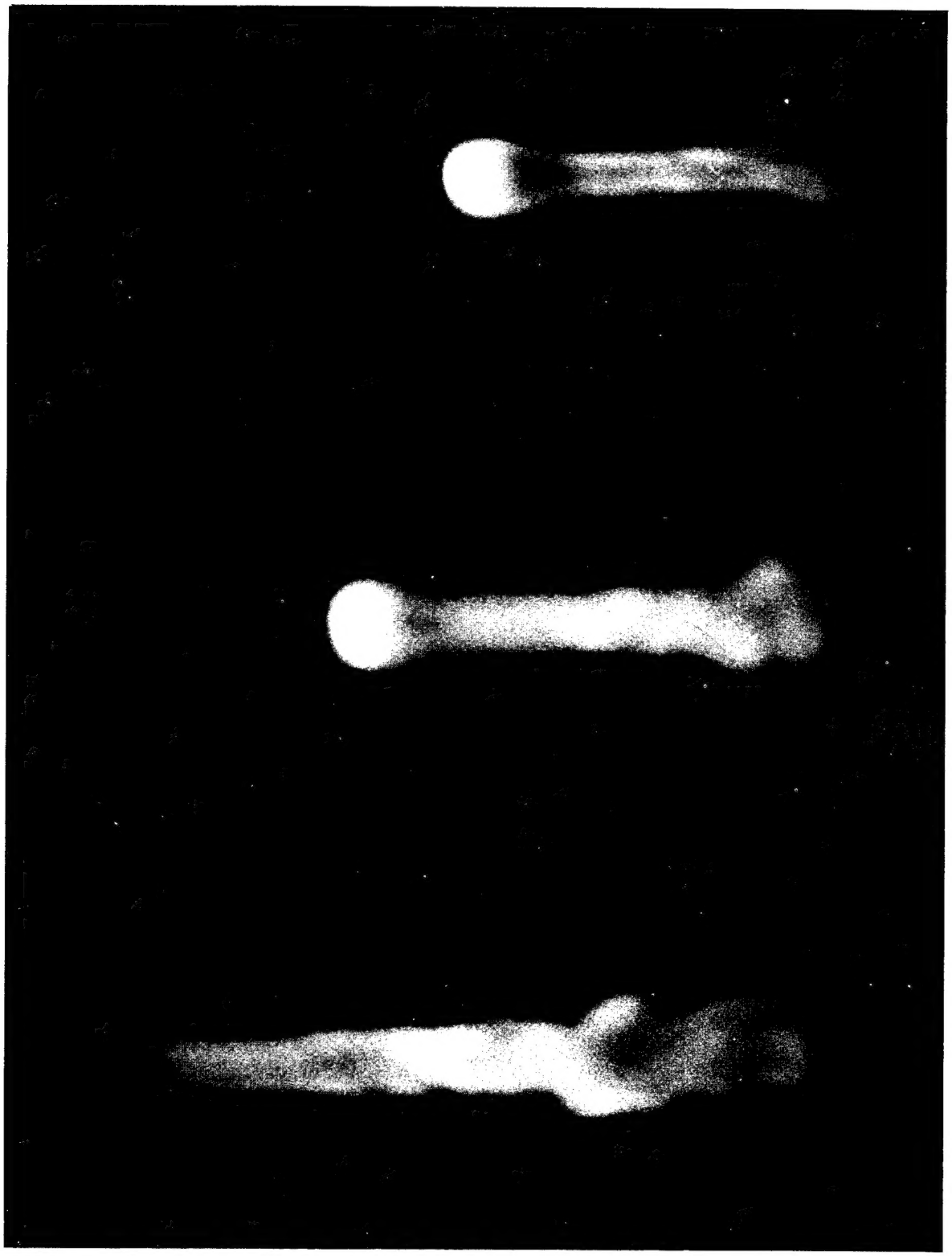

A-30236

Figure 14.- Successive photographs of luminous flow surrounding and in wake of polyethylene model; $Re_\infty = 68{,}400$; $U_\infty = 7.8$ km/sec; $\rho_\infty/\rho_o = 0.02$.

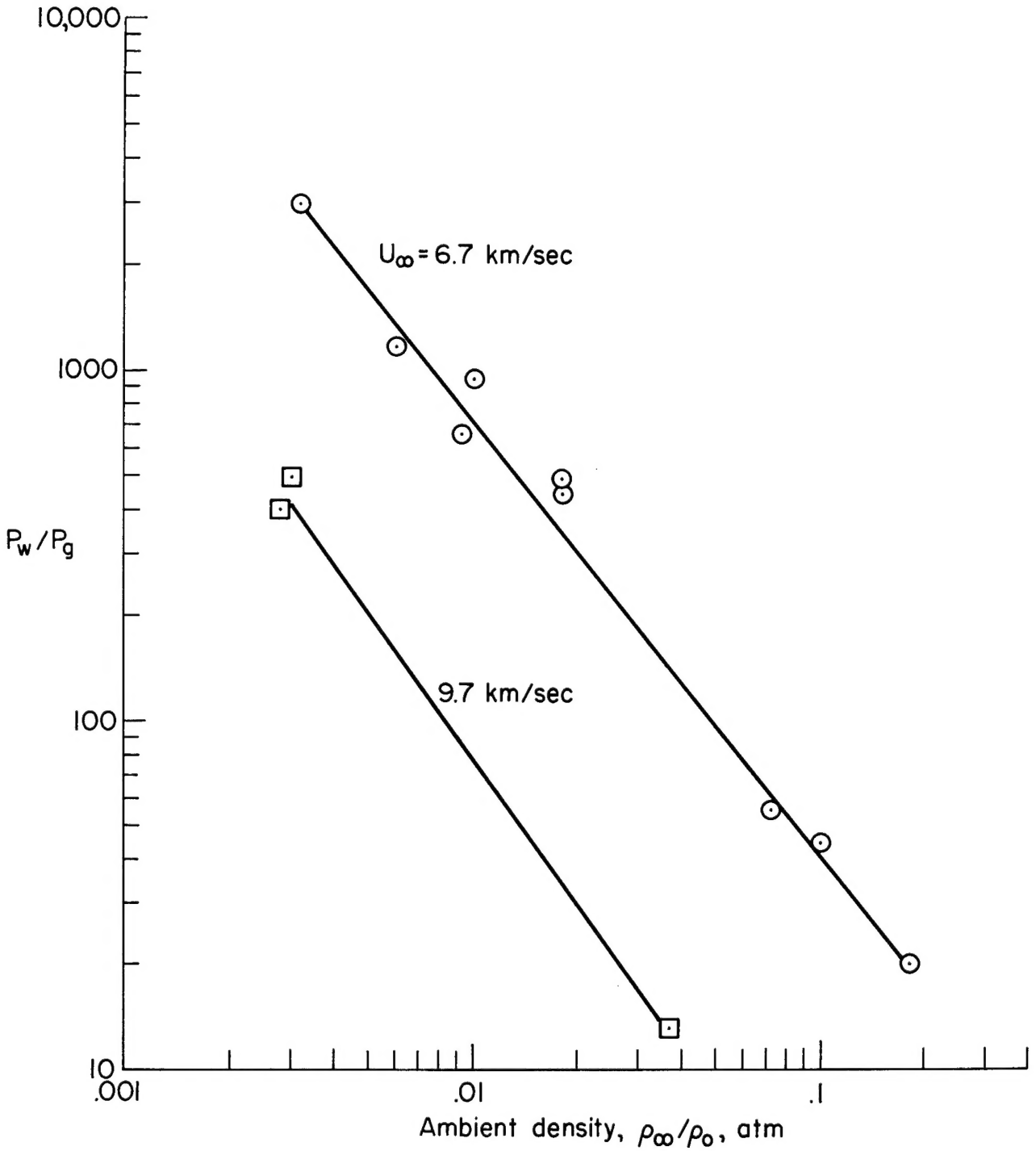

Figure 15.- Ratio of total wake radiative power to total power from equilibrium air in the model gas-cap polycarbonate; D = 0.71 cm.

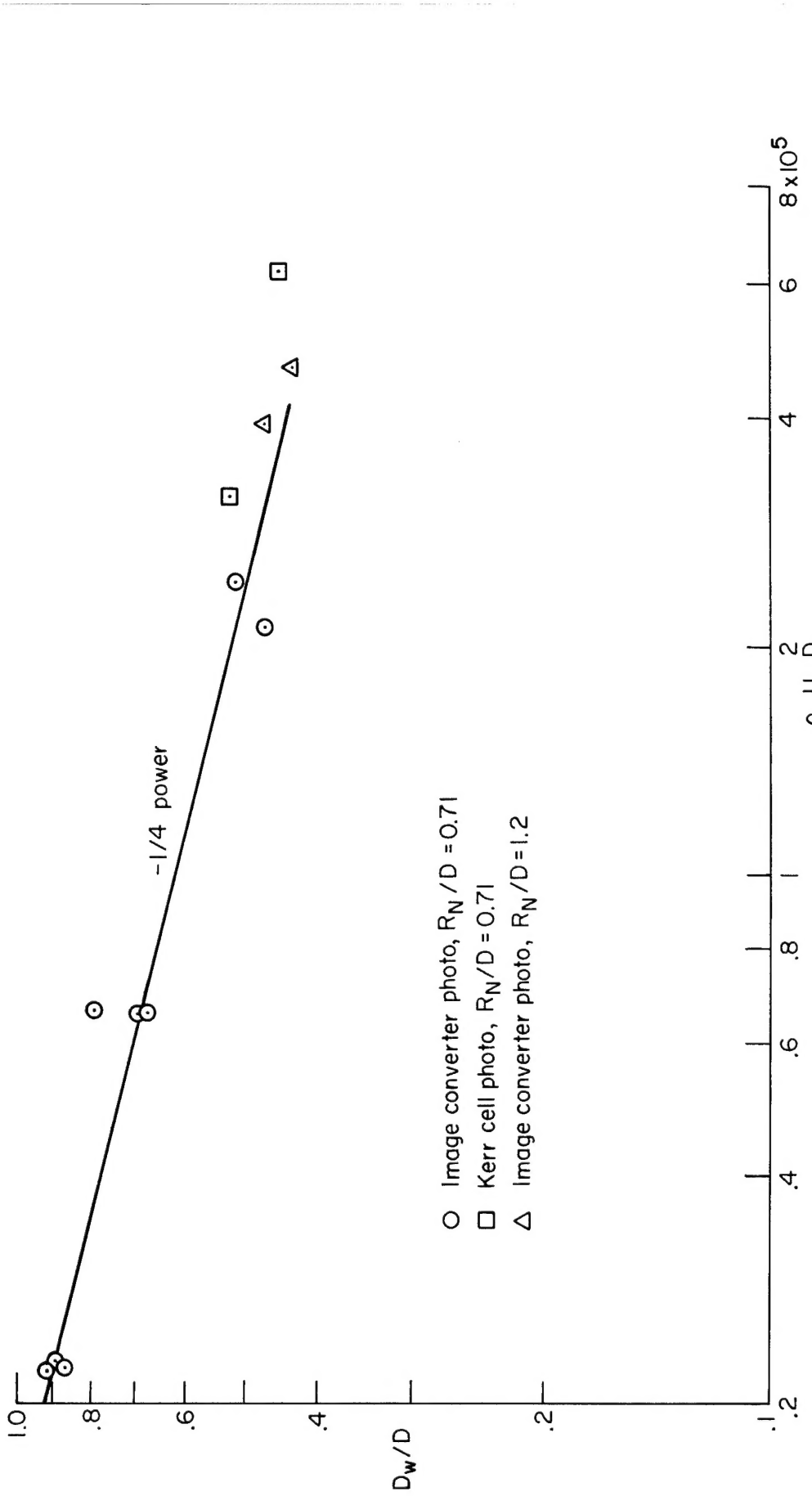

Figure 16.- Minimum diameters of luminous wakes.

NASA-Langley, 1965 A-853

"The aeronautical and space activities of the United States shall be conducted so as to contribute . . . to the expansion of human knowledge of phenomena in the atmosphere and space. The Administration shall provide for the widest practicable and appropriate dissemination of information concerning its activities and the results thereof."

—NATIONAL AERONAUTICS AND SPACE ACT OF 1958

NASA SCIENTIFIC AND TECHNICAL PUBLICATIONS

TECHNICAL REPORTS: Scientific and technical information considered important, complete, and a lasting contribution to existing knowledge.

TECHNICAL NOTES: Information less broad in scope but nevertheless of importance as a contribution to existing knowledge.

TECHNICAL MEMORANDUMS: Information receiving limited distribution because of preliminary data, security classification, or other reasons.

CONTRACTOR REPORTS: Technical information generated in connection with a NASA contract or grant and released under NASA auspices.

TECHNICAL TRANSLATIONS: Information published in a foreign language considered to merit NASA distribution in English.

TECHNICAL REPRINTS: Information derived from NASA activities and initially published in the form of journal articles.

SPECIAL PUBLICATIONS: Information derived from or of value to NASA activities but not necessarily reporting the results of individual NASA-programmed scientific efforts. Publications include conference proceedings, monographs, data compilations, handbooks, sourcebooks, and special bibliographies.

Details on the availability of these publications may be obtained from:

SCIENTIFIC AND TECHNICAL INFORMATION DIVISION

NATIONAL AERONAUTICS AND SPACE ADMINISTRATION

Washington, D.C. 20546